Research Article

Mohammad Afzal, Sher Ullah, Nasir Assad, Muhammad Naeem-ul-Hassan*, Maria Kanwal, Bakhtawar Mubashar, Roeel Shahzad, Muhammad Nauman Khan, Muhammad Ammar Javed, Sana Wahab, Baber Ali, Muhammad Adnan, Alevcan Kaplan*, Muhammad Hassan Sarfraz*, Jawaher Alkahtani, and Imane Mehdaoui

Photocatalytic degradation of organic dyes and biological potentials of biogenic zinc oxide nanoparticles synthesized using the polar extract of *Cyperus scariosus* R.Br. (Cyperaceae)

https://doi.org/10.1515/gps-2024-0038
received February 18, 2024; accepted March 06, 2024

Abstract: In this study, the polar root extract of *Cyperus scariosus* R.Br. was used for the biogenic synthesis of ZnO NPs. The results of this study show that ZnO NPs have a spherical structure with an average size of 85.4 nm. The synthesized catalysts were tested for their photocatalytic activity by degrading methyl orange and methylene blue under sunlight. Improved degradation efficiencies of 79.44% and 84.92% were achieved within 120 min. ZnO NPs exhibited strong antibacterial activity against both Gram-positive *Listeria monocytogenes* (18 mm) and *Staphylococcus epidermidis* (20 mm) and Gram-negative strains of *Escherichia coli* (16 mm) and *Bordetella bronchiseptica* (14 mm), as shown by the inhibition zones, which were comparable to the positive control (ceftriaxone) but larger than the plant root extract. ZnO NPs showed high antioxidant activity, as a ferric-reducing antioxidant power assay value of 66.29 µg (AAE µg·mL^{-1}) and a DPPH value of 57.44 µg (AAE µg·mL^{-1}) were obtained at a concentration of 500 µL, which was higher than those of the *C. scariosus* root extract. Quantification of the total phenolic and flavonoid content yielded values of 57.63 µg (GAE µg·mL^{-1}) and 70.59 µg (QCE µg·mL^{-1}), respectively. At a concentration of 500 µL (1 mg·mL^{-1}), the tested nanoparticles (NPs) showed a greater anti-inflammatory effect (84.12%) compared to the root extract of *C. scariosus* (34.39%). Overall, our findings highlight the versatile properties of green synthesized ZnO NPs and demonstrate their potential for environmental remediation and antimicrobial formulations, as well as promising candidates for further investigation in biomedical fields such as drug delivery and therapy.

*** Corresponding author: Muhammad Naeem-ul-Hassan,** Institute of Chemistry, University of Sargodha, Sargodha 40100, Pakistan, e-mail: sobheel@yahoo.com
*** Corresponding author: Alevcan Kaplan,** Department of Crop and Animal Production, Sason Vocational School, Batman University, Batman, 72060, Turkey, e-mail: kaplanalevcan@gmail.com
*** Corresponding author: Muhammad Hassan Sarfraz,** Botnar Institute of Musculoskeletal Sciences, Nuffield Department of Orthopaedics, Rheumatology and Musculoskeletal Sciences, University of Oxford, OX3 7LD, United Kingdom, e-mail: muhammad.sarfraz@ndorms.ox.ac.uk
Mohammad Afzal: Institute of Chemistry, University of Sargodha, Sargodha 40100, Pakistan, e-mail: kmohammadafzal19@gmail.com
Sher Ullah: Institute of Chemistry, University of Sargodha, Sargodha 40100, Pakistan, e-mail: sheri66986@gmail.com
Nasir Assad: Institute of Chemistry, University of Sargodha, Sargodha 40100, Pakistan, e-mail: nakhan_98@yahoo.com
Maria Kanwal: Institute of Chemistry, University of Sargodha, Sargodha 40100, Pakistan, e-mail: mariakanwal865@gmail.com
Bakhtawar Mubashar: Institute of Chemistry, University of Sargodha, Sargodha 40100, Pakistan, e-mail: bakhtawarmubashar@gmail.com
Roeel Shahzad: Institute of Chemistry, University of Sargodha, Sargodha 40100, Pakistan, e-mail: rueelshehzad@gmail.com
Muhammad Nauman Khan: Department of Botany, Islamia College Peshawar, Peshawar 25120, Pakistan, e-mail: nomiflora@uop.edu.pk
Muhammad Ammar Javed: Institute of Industrial Biotechnology, Government College University, Lahore 54000, Pakistan, e-mail: ammarjaved94@gmail.com
Sana Wahab: Department of Plant Sciences, Quaid-i-Azam University, Islamabad 45320, Pakistan, e-mail: sanawahab1995@gmail.com
Baber Ali: Department of Plant Sciences, Quaid-i-Azam University, Islamabad 45320, Pakistan, e-mail: baberali@bs.qau.edu.pk
Muhammad Adnan: Department of Chemistry, Islamia College Peshawar, Peshawar 25120, Pakistan, e-mail: muhammadadnan112255@gmail.com
Jawaher Alkahtani: Department of Botany and Microbiology, College of Science, King Saud University, Riyadh 11451, Saudi Arabia, e-mail: jsalkahatani@gmail.com
Imane Mehdaoui: Laboratory of Electrochemistry, Modelization and Environment Engineering, Faculty of Science Dhar El MAhraz, Sidi Mohamed Ben Abdellah University, Fez 30000, Morocco, e-mail: mehdaouiimane2@gmail.com

Keywords: antibacterial, anti-inflammatory, antioxidant, biogenic synthesis, photocatalytic degradation, zinc oxide nanoparticles

1 Introduction

Metal oxide semiconductors and their corresponding nanocomposites have attracted great attention worldwide due to their extraordinary chemical, physical, optical, magnetic, and electrochemical properties [1,2]. Nanoscale materials have improved properties compared to their bulk counterparts. Metal-based nanomaterials exhibit extraordinary properties due to their remarkably small dimensions, often between 1 and 100 nm [3–6]. This is mainly due to the fact that nanomaterials have a high surface-to-volume ratio [7,8]. Nano-sized materials are used in many fields due to their valuable properties, e.g., in antimicrobial [8,9], water treatment, medicine, drug delivery, solar cells, agriculture [10], food industry, textile industry, electronics, catalysis, cosmetics [11–13], colorimetric sensing [14], environmental remediation [15], and as antioxidants [16]. Metal oxide nanoparticles (NPs) have significant chemical and physical properties that make them widely applicable in various fields of scientific research and technological applications [17,18].

Industrial organic dyes have recently become a major global problem as they pollute polluting water supplies. The problem of water pollution not only hinders the progress of human society but also the advancement of industrial technology [19]. Consequently, the effort to reduce water pollution is of utmost importance to researchers. In particular, methylene blue (MB) and methyl orange (MO) are among the organic photoactive dyes that belong to the heterocyclic aromatic chemical complexes and are widely used as coloring substances in the textile, printing, dyeing, leather, pharmaceutical, and cosmetic industries [20,21]. Previous research on MB and MO has shown that dyes are harmful to marine life and cause major ecological problems [22]. Therefore, these industries are now facing the urgent challenge of completely removing MB, MO, and related heterocyclic organic pollutants from wastewater. Previous studies have shown that dye waste products can be effectively degraded using various remediation methods, such as electrochemical degradation, adsorption solar photo-Fenton degradation, and photocatalysis [23], [24,25]. Photocatalytic degradation is an effective and cost-effective approach for water treatment that uses solar energy to break down organic dye pollutants into non-toxic chemicals [26]. Organic dyes in industrial wastewater have been degraded using a variety of semiconductors or composites [27,28]. Zinc oxide nanoparticles (ZnO NPs) have attracted much attention among semiconducting metal oxides (NPs) due to their many attractive properties, such as their large surface area, wide band gap, long-lasting chemical stability, and low ecological effects [29]. Semiconductors based on zinc oxide (ZnO) are used in fields as diverse as electronics, sensing, optical materials, photovoltaic cells, and photoelectronics. In addition to its many other useful properties, zinc oxide (ZnO) NPs are used extensively for the photodegradation of organic dyes in wastewater [30].

ZnO NPs have gained considerable attention in the field of metal oxide NPs due to their low cost, high safety standards, and ease of fabrication [31]. ZnO NPs possess significant semiconducting properties due to their considerable band gap of 3.37 eV [32]. The formation of ZnO NPs is affected by chemical, physical, and biological factors. The physical synthesis requires the use of a high vacuum and high energy consumption, while the chemical processes are not very environmentally friendly. Consequently, the biogenic synthesis method is gaining recognition due to its environmentally sustainable, economically viable, and safe nature. The green synthesis method for NPs involves the use of plant extracts, bacterial cultures, fungal cultures, and algae extracts. The plant extracts have considerable potential as a source of phytochemicals as they contain a variety of phytochemical classes, including polyphenols, terpenoids, flavonoid alkaloids, and sugars [33]. Most of these phytochemicals extracted in polar solvents are polar in nature and play an important role in the synthesis of NPs [34]. These compounds serve as reducing agents as well as capping or stabilizing agents. ZnO NPs have already been successfully synthesized from various plant parts, such as roots, stems, seeds, leaves, peels, and fruits [35,36]. The overall composition of the bioactive substances in the plant extracts varies greatly, and the reaction conditions, such as the extract and zinc concentrations, temperature, heating time, and pH, determine the final properties of these NPs. One of the major challenges is to explore the mechanism by which the biogenic synthesis of ZnONPs occurs in order to control the morphology of the synthesized NPs and to achieve a better understanding of the involved chemical phenomena for the desired applications [37].

The primary objective of the present work was to investigate the potential use of biogenically synthesized ZnO NPs using the polar root extract of *C. scariosus*, a member of the Cyperaceae family. This plant has been associated with several biological benefits, including antibacterial, anti-diabetic, anti-inflammatory, antihypertensive, and antioxidant properties [38]. The synthesized ZnO NPs were subjected to spectroscopic and microscopic techniques, such as Fourier-transform infrared spectroscopy, UV-Vis spectroscopy, energy-

dispersive X-ray spectroscopy, scanning electron microscopy (SEM), dynamic light scattering (DLS), X-ray diffraction (XRD), and zeta potential measurements. The biogenically synthesized ZnO NPs were investigated for their photocatalytic, antibacterial, anti-inflammatory, and antioxidant properties according to standard protocols.

2 Experimental methods

2.1 Materials

A sample of the roots of *C. scariosus* was purchased from a local market in Sargodha, Pakistan, and checked by the botanist of the Department of Botany, University of Sargodha, Punjab, Pakistan. *n*-Hexane (Sigma-Aldrich® Germany), ethanol (99.8%) (Sigma-Aldrich® Germany), zinc acetate (ZnOAC) (Sigma-Aldrich® Germany), DPPH (Sigma-Aldrich® Germany), Folins–Ciocalteu phenol reagent (Sigma®) and diclofenac sodium (Acros Organics, Thermo Fisher Scientific US). All chemicals and solvents used in this research were of analytical grade and did not require further purification. Deionized water (DH_2O) was used to prepare the solutions. Bacterial strains and Mueller–Hinton agar (Bio-Rad US) were obtained from the Biochemistry Laboratory, Institute of Chemistry, University of Sargodha, Pakistan.

2.2 Extraction of polar extract

The polar extract from the tuberous root of *C. scariosus* was extracted using a conventional method following the protocol of previous studies [13,39]. The tuberous roots were purified with DH_2O and then air-dried at 25°C in the shade for 15 days. The dried root was then crushed using a grinder, and the powder was sieved through a sieve with a mesh size of 75 µm. The powder solution (1 g per 20 mL) was then stirred for 5 h at room temperature using a hot plate stirrer. Whatman filter paper No. 40 was used to filter for filtering the solution, and the resulting filtrate was then rinsed with *n*-hexane. The treatment with *n*-hexane led to the separation of the polar and non-polar layers. The polar layer was then spread on a Petri dish and exposed to a temperature of 45°C for 24 h. After 24 h period, the polar extract was sealed in an Eppendorf tube and stored in the refrigerator for further use.

2.3 Phytochemical analysis

The polar extract of *C. scariosus* was analyzed for phytochemicals according to the method used by De Silva et al. Different compounds, such as alkaloids (detected using the Wagner test), flavonoids (identified by the lead acetate test), glycosides (confirmed by the sodium hydroxide test), lignins (detected by the Labat test), saponins (identified by the foam test), coumarins (identified with the sodium hydroxide test), phenols (identified with the ferric chloride test), sterols (identified with the Salkowiski test), leucoanthocyanin (identified with the isoamyl alcohol test), and fatty acids (identified with the Mojonnier method) were present [40].

2.4 Green synthesis of *C. scariosus*-mediated ZnO NPs

ZnO NPs were prepared according to the methodology described in the study of Ghaffar et al. [13], with some modifications. About 100 mL of aqueous solution of 0.68 g ($Zn(CH_3CO_2)_2$) was prepared in a 250 mL volumetric flask. The *C. scariosus* extract solution (20 mL) was mixed with the zinc acetate solution, and the mixture was frequently stirred for about 30 min. The solution was then heated at 70°C for 20 min with constant stirring until a brown precipitate was formed. The brown precipitate was then rinsed off with ethanol and DH_2O. The product was washed and then calcined at 450°C. The ZnO NPs were synthesized in green using the above method. The synthesized ZnO NPs were sealed in an Eppendorf tube labeled as ZnO NPs.

2.5 Characterization

The investigation and characterization of the biogenic ZnO NPs were performed using a UV-visual spectrophotometer (UV-1700 Pharmspec, Shimadzu, Japan) in the wavelength range of 700–300 nm. The extract from the polar root of *C. scariosus* extract and the green synthesized ZnO NPs were subjected to Fourier transform infrared spectroscopy (FTIR) in the range of 4,000–500 cm^{-1} using KBr pellets to identify the elongation of functional groups. The crystal size of the biosynthesized ZnO NPs was measured by XRD (JDX-3532, JEOL, Tokyo, Japan). XRD measurements were performed at 2θ angles ranging from 10 to 80° using CuKα radiation (λ = 1.55056). The device was operated with an

accelerating voltage of 40 kV and a current of 15 mA. An SEM (EDX, JEOL EDX system japan) with 20 kV operating voltage was used to analyze the elemental composition and surface morphology of the ZnO NPs. The physical dimension of the nanocrystals was determined using a Malvern Zetasizer Nano ZS (United Kingdom). The evaluations were carried out at a wavelength of 633 nm using a He-Ne diode. A Whatman filter with a particle size of 0.2 m was used to filter the liquid sample to remove solid impurities. The 10 mm long section contains the filtrate, which was placed in a microcuvette. The sample was exposed to a temperature of 25°C for 2 min before analysis. The average variances were given for the number of analyses. The surface charge of the biosynthesized ZnO NPs was measured using the zeta potential technique and Malvern's Zetasizer.

2.6 Photocatalytic activity

The dyes MO and MB have unique physical and chemical properties with the structural formulas shown in Figure 1. The melting point of MB is around 100–110°C, and the boiling point is over 200°C. The melting point of MO is around 190–192°C, and the boiling point is above 200°C. In interaction with carboxymethyl cellulose (CMC), MB has a strong adsorption capacity, reaching over 300 $mg{\cdot}g^{-1}$ [41]. However, in combination with bimetallic Fe-CdO NPs, MO is rapidly degraded; after UV irradiation, the percentage of degradation is 93.44 for MO alone and 88.29% for MO in a binary dye combination. It was also shown that nanocrystalline molybdenum oxide (MoO_3) uses its photocatalytic activity to effectively degrade MB. After 90 min, the degradation efficiencies were 56.15% for $Mo_{17}O_{47}$ and 95.78% for α-MoO_3 [42].

To determine the photocatalytic activity of ZnO NPs, 30 mL of MB and MO, 10 ppm each, were first mixed with 30 mL of the catalyst (1 $mg{\cdot}mL^{-1}$), according to the protocol of Ghaffar et al. [13]. The dye solutions were stirred in the dark for 30 min to determine the maximum amount of MB and MO that the photocatalyst could absorb. About 5 mL of each solution was collected and centrifuged to extract the catalyst particles after being exposed to sunlight for 2 h. The investigations were conducted between 10 am and 2 pm on clear, sunny days (UV to IR, UV index between 7 and 10, measured with a mobile app). UV-Vis spectrophoto meter measurements (Shimadzu UV-1800 spectrophoto meter) were used to quantify the residual dye solution. UV measurements were performed in triplicate with a maximum difference of 5% between individual measurements. The concentration of dyes in the solution was determined by analyzing the absorption peaks of MO at 460 nm and MB at 665 nm. The percentage degradation rate was calculated using the following equation:

$$\text{Degradation efficacy}(\%) = C_0 - C/C_0 \times 100 \quad (1)$$

where C_0 is the absorption of the dyes in the time interval zero, and C is the absorption of the dyes at different time intervals in the presence of sunlight.

2.7 Antibacterial activity

The evaluation of the antibacterial potential of the biogenically synthesized ZnO NP*s* was performed according to the procedure of Khan et al. [16], with some modifications. A solution was prepared by mixing 6.3 g of Mueller-Hinton agar in 120 mL of DH_2O. The agar-Petri plate mixture was then autoclaved at 121°C with a pressure of 15 psi for approximately 20 min. After the sterilization process, 20 mL of Mueller-Hinton agar solution was added to each Petri dish, which then solidified for 20 min. Using the sterilized media, the pure cultures were subcultured at 37°C using an orbital shaker at 200 rpm. The bacterial strains *Listeria monocytogenes* (ATCC 13932), *Staphylococcus epidermidis* (ATCC 12228), *Escherichia coli*

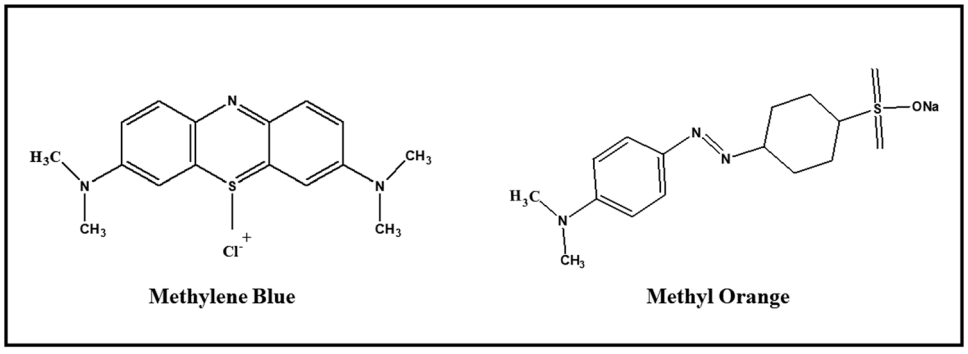

Figure 1: Chemical structure of MB and MO.

(ATCC 10536), and *Bordetella bronchiseptica* (ATCC 4617) were inoculated into each Petri dish using the stick/spread plate technique. A total of four wells were made with a cork borer and then labeled alphabetically. About 30 µL of the positive control ceftriaxone sodium (1 mg·mL^{-1}) was added together with 30 µL of ZnO NPs (1 mg·mL^{-1}), 30 µL (1 mg·mL^{-1}) of plant extract, and a negative control consisting of deionized water (DH_2O). The Petri dishes were then placed in an oven at 37°C for 24 h. The entire procedure took place in a laminar flow cabinet in a clean and sterilized laboratory environment.

The minimum inhibitory concentration (MIC) of the green synthesized ZnO NPs was measured according to the standard procedure defined by the Clinical and Laboratory Standards Institute [43]. In this study, both Gram-positive and Gram-negative strains were used to determine the MIC. Four bacterial strains, namely *Listeria monocytogenes* (ATCC#13932), *Staphylococcus epidermidis* (ATCC#12228), *Escherichia coli* (ATCC#10536), and *Bordetella bronchiseptica* (ATCC#4617), were cultured in a shaking incubator at a temperature of 37°C and a shaking speed of 200 rpm for 24 h. Bacteria were cultured in a Mueller incubator at a temperature of 37°C and a shaking speed of 200 rpm. The bacteria were grown in a Mueller Hinton broth medium. The concentration of bacterial inoculum was adjusted to 105 CFU·mL^{-1}. The MIC of the ZnO NPs was determined using the conventional broth microdilution technique. A solution containing the synthesized ZnO NPs at a concentration of 1 mg·mL^{-1} was prepared to determine the MIC. The MIC was determined by a series of diluted concentrations between 100 and 10 µg·mL^{-1}. In addition, positive control tests with simple bacterial strains and broth and negative control tests with ZnO NPs (100 µg·mL^{-1}) were performed. The tubes were thereafter placed in an incubator at 37°C for 24 h. After incubation, the concentration of ZnO NPs at which bacterial growth was completely inhibited was determined.

2.8 Antioxidant activity

2.8.1 Ferric reducing antioxidant power (FRAP) assay

The methods described in previous studies [44,45] were used with some modifications for the FRAP assay. In brief, solutions of ZnO NPs were prepared at concentrations ranging from 100 to 500 µg·mL^{-1}. The solutions were prepared by mixing 2.5 mL of a sodium phosphate buffer solution (0.2 M) with a pH of 6.6 with a 1% aqueous solution of potassium ferricyanide and incubating the mixture at 50°C for 20 min. The process was finally stopped by adding a 10% (w/v) solution of trichloroacetic acid (TCA) to the mixture. The solution was then centrifuged for 10 min at a speed of 3,000 rpm. A 0.1% ferric chloride solution was added to the mixture, along with 2.5 mL of DH_2O. A spectrophotometer (UV-1700 Pharmspec, Shimadzu) was used to determine the absorbance at 700 nm. The antioxidant potential of FRAP was determined using the following equation. The scavenging activity was estimated using the following equation [46]:

$$x = y/0.0027, \quad R^2 = 0.9801 \tag{2}$$

2.8.2 2,2-Diphenyl-1-picrylhydrazyl (DPPH) assay

The DPPH scavenging activity of the biogenically synthesized ZnO NPs was evaluated using the protocol described by Khan et al. [16] with some modifications. Various amounts of green-synthesized ZnO NPs (100–500 µg·mL^{-1}) were mixed with 3 mL of ethanolic DPPH solution (4 mg per 100 mL), and ethanol (99.8%) was added to each sample to increase the final volume to 10 mL. The solutions were then incubated for 30 min at room temperature and in the dark. After that, absorbance at 517 nm was then measured for both the test sample and the reference sample (ascorbic acid). The assessment of the percentage scavenging activity of the antioxidant (DPPH) was performed by using the following equation (Eq. 3) [47]:

$$\begin{aligned} &\%\text{Scavenging activity} \\ &= (\text{Ac 517 of control} - \text{As 517 of sample}) \\ &\quad /\text{Ac 517 of control} \times 100 \end{aligned} \tag{3}$$

where Ac is the absorbance of the control and As is the absorbance of the sample.

2.8.3 Total polyphenol content (TPC)

The Folin–Ciocalteu method, as described by Do et al. [48], was used with some modifications to evaluate the total polyphenol content. Initially, 2 mL of DH_2O was added to 250 µL of a 1 N solution of Folin–Ciocalteu phenol, along with different volumes (100–500) µL (1 mg·mL^{-1}) of ZnO NPs. The resulting mixture was then incubated for 8 min at room temperature in the dark. Then, 750 µL of a 20% sodium carbonate solution (Na_2CO_3) and 950 µL of DH_2O were added. After incubation for 30 min in the absence of light, the absorbance of the solutions was quantified at a wavelength of 765 nm using a Shimadzu UV-1800 spectrophotometer. The results were expressed as (µg (GAE µg·mL^{-1})) of the ZnO NP sample. The scavenging activity of TPC was analyzed using the following equation [46]:

$$x = y/0.0019, \quad R^2 = 0.9659 \tag{4}$$

2.8.4 Total flavonoid content (TFC)

The TFC was estimated according to the methodology described by Do et al. [48] with some modifications. A colorimetric protocol was used, which included the use of aluminum chloride ($AlCl_3$) to quantify flavonoid content in the tested sample. In summary, 100 and 500 µL (1 mg·mL^{-1} concentration) of ZnO NPs were mixed with 0.75 mL of methanol, and the resulting mixture volume was increased to 2 mL by adding DH_2O. Then, 300 µL of a solution containing 5% sodium nitrate and 300 µL of a solution containing 10% $AlCl_3$ were added to each sample, and the samples were incubated at 37°C for 10 min. Subsequently, 2 mL of a 1 mol·L^{-1} sodium hydroxide (NaOH) solution was added, and the total volume was increased to 5 mL with DH_2O. The solution was then incubated for 40 min at room temperature. After incubation, the absorbance was measured using a Shimadzu UV-1800 spectrophotometer at 510 nm. TFC of the experimental results was obtained using quercetin as a reference standard, and the measurements were expressed as mg quercetin equivalent per gram (mg QCE·g^{-1}) of ZnO NPs. The percent scavenging activity of TFC was measured using the following equation [46]:

$$x = y/0.0022, \quad R^2 = 0.9883 \tag{5}$$

2.9 Anti-inflammatory activity

2.9.1 Inhibition of protein denaturation

The protein denaturation methods described in previous studies [16,49] were used with some minor modifications to evaluate the anti-inflammatory properties of green synthesized ZnO NPs. The solutions of green synthesized ZnO NPs were prepared in the range of 100–500 µL·mL^{-1} (1 mg·mL^{-1}). Phosphate-buffered saline (PBS) with a pH of 6.4 and a freshly prepared egg-albumin mixture (0.2 mL) were added to the solutions of the green synthesized ZnO NPs to prepare the final mixture. The final volume of the solution was brought to 5 mL by adding DH_2O. The solution was incubated at 37°C for 20 min. In a further step, the samples were exposed to a temperature of 70°C for 5 min after incubation. Following the procedure described above, a standard reference solution of diclofenac sodium with a concentration of 500 µL·mL^{-1} (1 mg·mL^{-1}) was used to measure the absorbance. A Shimadzu UV-1800 spectrophotometer (Shimadzu UV-1800 spectrophotometer) was set at 660 nm to obtain accurate results for turbidity measurements. A phosphate buffer and egg albumin were used to prepare a blank solution, and the denaturation of the protein was determined according to the following equation [50]:

$$\text{Inhibition of protein denaturation}(\%) = (\text{A660 of Sample/A660 of control} - 1) \times 100 \tag{6}$$

2.10 Statistical analysis

All samples were analyzed in at least triplicate, and the results were presented as mean ± standard deviation. Statistical analysis was performed using Office Excel and Origin 2021.

3 Results and discussion

3.1 Phytochemical screening

A phytochemical study confirmed the presence of numerous phyto-constituents, as shown in Table 1. The findings indicate that the plant extract includes many significant phytochemicals, such as phenols and flavonoids, which play a role in the formation of NPs. These chemical groups play a key role in the green synthesis of ZnO NPs and act as reducing and stabilizing agents. The hydroxyl groups present in phenols and flavonoids are used to reduce and stabilize zinc ions, leading to the formation of ZnO NPs [51].

3.2 Green synthesis of ZnO NPs

Mechanisms for the plant-mediated synthesis of NPs have been proposed in several studies, and examples of the proposed mechanisms are shown in Figure 2. In general, the

Table 1: Phytochemical screening of *C. scariosus* extract (+ positive, − negative)

Test	Result
Flavonoids	+
Alkaloids	+
Glycosides	−
Lignin	−
Phenols	+
Coumarins	−
Saponins	+
Sterols	+
Leucoanthocyanin	−
Fatty acid	−

Samples were analyzed at least in triplicate, and results are presented as mean ± standard deviation.

phytochemicals present in the plant extract facilitate the conversion of aqueous Zn salt precursors to Zn through a reduction reaction. Subsequently, oxygen is supplied during the calcination process, while some phytochemicals contribute to the stabilization of the synthesized NPs. The second hypothesis states that the phytochemicals and Zn^{2+} form a complex that is hydrolyzed to generate $Zn(OH)_2$ and finally calcined to produce ZnO NPs [52].

Herein, the synthesis of ZnO NPs was carried out in a two-step procedure, as described in a previously published methodology by [13]. Initially, $Zn(OH)_2$ was prepared from ($Zn(CH_3CO_2)_2$), followed by calcination of this intermediate at 450°C to obtain ZnO NPs. The potential process of Zn reduction is the utilization of phytochemicals, especially polyphenols and flavonoids, present in the polar extract [53]. These phytochemicals help in the separation of Zn ions from their solvating anionic counterparts. Subsequently, the Zn ions are reduced, which is facilitated by chelation with the phytochemicals and leads to the formation of more stable metallic Zn. The appearance of $Zn(OH)_2$, a precipitate with a white, milky appearance, results from the binding of the hydroxyl group (OH) of the phytochemicals to Zn^{2+} [54]. The intermediate was heated and dried at 70°C for 6 h and, then calcinated at 450°C to produce ZnO NPs. It has been shown that the presence of polyphenols in *C. scariosus* is characterized by the abundance of hydroxide groups (OH). Hydroxide groups are responsible for the reduction of ($Zn(CH_3CO_2)_2$) to $Zn(OH)_2$, which is due to the moderate chemical interactions between antioxidants and the metal halide. Spectroscopic and microscopic methods were used to investigate the biogenically synthesized ZnO NPs mediated by the root extract of *C. scariosus*. The antibacterial, anti-inflammatory, and antioxidant effects of biogenic ZnO NPs synthesized from *C. scariosus* root extract are described in more detail.

3.3 UV-Vis spectroscopy of ZnO NPs

The absorption spectra of the ZnO NPs in suspension were analyzed using a UV-Vis spectrophotometer to determine the optical properties of these eco-friendly NPs (Figure 3(a)). The presence of a distinct peak at around 366 nm in the spectrum confirmed the synthesis of ZnO NPs at the nanoscale, which is also consistent with previous studies [54,55]. The localized surface plasmon resonance (LSPR) of NPs is responsible for the appearance of this peak. The occurrence of this peak can be attributed to the excitation of free electrons [51]. These oscillations occur when the NPs are aligned with the spectrum of the incident radiation. The results of our study are in close agreement with the previously documented literature [51,56].

The analysis of UV-Vis spectroscopy data using the Tauc equation (Eq. 7) was applied to determine the optical band gap (E_g) of the biogenically synthesized ZnO NPs:

$$(\varepsilon h\nu)^2 = K(h\nu - E_g) \tag{7}$$

Here, h is Planck's constant, a fundamental constant of quantum mechanics, ν is the frequency, and ε is the molar extinction coefficient, a property for quantifying the absorption of light by a substance. In addition, K is an energy-

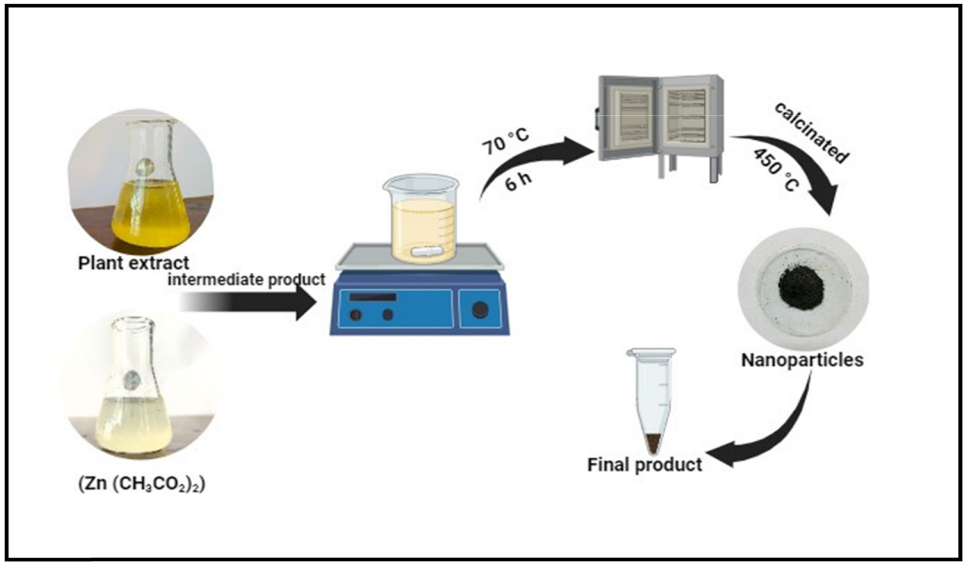

Figure 2: Schematic mechanism of the formation of ZnO NPs with the extract of *C. scariosus*.

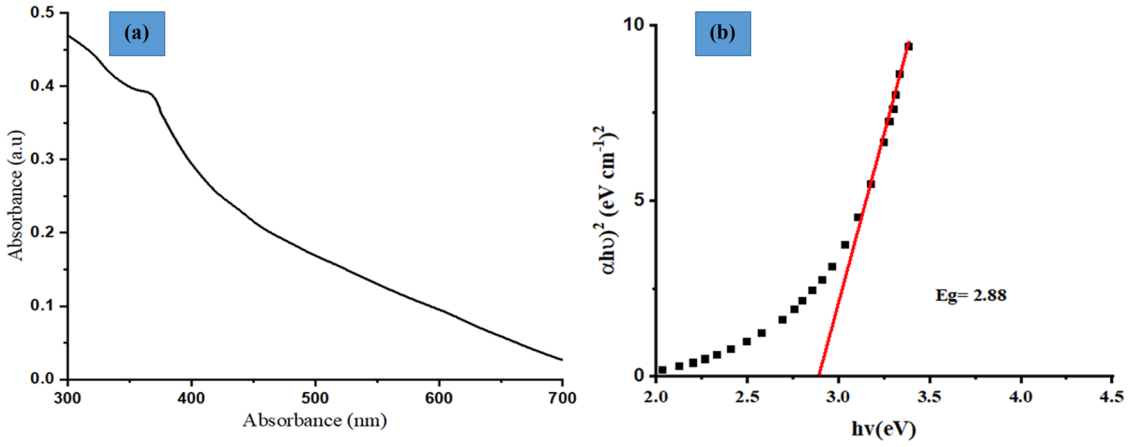

Figure 3: (a) UV-Vis spectra of the biogenically synthesized ZnO NPs and (b) band gap energy (E_g) of the biogenically synthesized ZnO NPs using *C. scariosus* root extract.

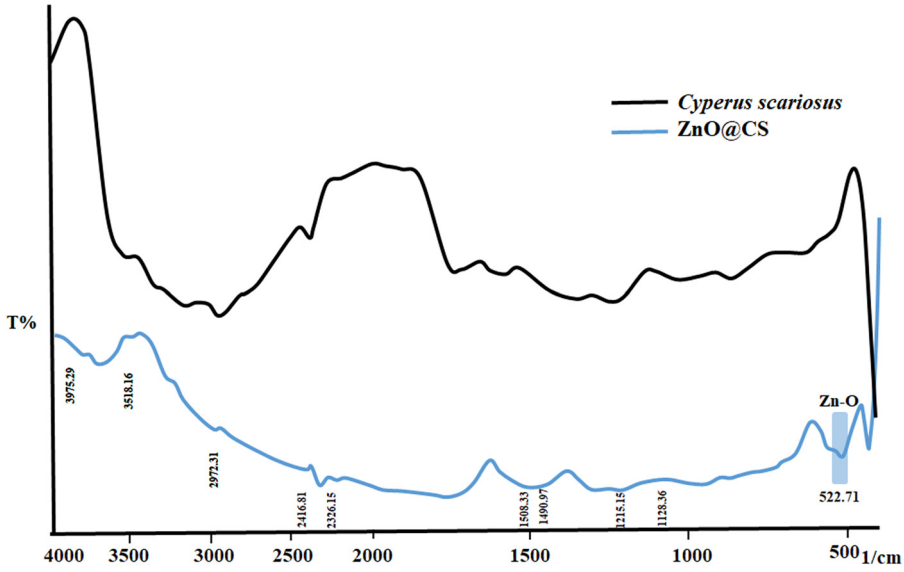

Figure 4: FTIR spectra of *C. scariosus* root extract and ZnO NPs.

independent constant that remains constant regardless of the energy used. Finally, n is a parameter that depends on the type of displacement under consideration. In the case of materials with a direct allowed band gap, the parameter n is exactly equal to 2. The typical band gap was calculated by finding the convergence of the linear section of the graph of $(\varepsilon h\nu)^2$ against $h\nu$ indicated by the red line in Figure 3(b). An energy value of 2.88 eV was determined for the ZnO NPs, indicating a lower energy compared to bulk ZnO, which has an energy value of 3.37 eV [13]. As the band gap energy decreases, the NPs absorb more wavelengths of light, resulting in a blue shift in their absorption spectrum, and conversely, as the particle size decreases, the amount of energy required to absorb light decreases. The band gap energy of a semiconductor is the lowest energy required to transfer an electron from the valence band to the conduction band, and it is proportional to the maximum photon energy absorbed by the material [57]. By reducing the band gap energy, the NPs can absorb light at lower energies, resulting in greater light absorption [58].

3.4 FT-IR

FT-IR was used to investigate the elongation of the functional groups of the eco-friendly synthesized ZnO NPs. Figure 4 shows a representative FTIR spectrum of a pure plant extract and ZnO NPs, while Table 2 provides an absorption spectrum with potential functional group stretching. The absorption peak observed at 522.71 cm^{-1} corresponds to the pronounced absorption of the Zn–O

Table 2: Absorption spectrum with functional group stretching

Sr. No.	Frequency of ZnO NPs (cm^{-1})	Frequency of *C. scariosus* (cm^{-1})	Functional group
1	3,975.29	3,807.48	OH, stretching vibrations
2	3,518.16	3,464.15	Phenol
3	2,972.31	2,908.65	C–H stretch in alkanes
4	2,416.81	—	Carboxylic acid
5	2,326.15	2,315.23	C–N
6	1,508.33	1,573.91	C═C stretch in the aromatic ring and C═O stretch in polyphenols
7	1,490.97	—	C–N stretch of amide-I in protein
8	1,215.15	1,230.58	Alkyl ketone
9	1,128.36	—	Alkyl amine
10	522.71	—	Zn–O

bond, [59], while the extended stretching of 3,464.15 cm^{-1} observed at 3,518.16 cm^{-1} is due to the absorption of hydroxyl groups, which are mainly found in the structures of carbohydrates, tannins, and phenolic compounds [60].

3.5 XRD

XRD was used to validate the crystal structure and evaluate the purity phase of ZnO NPs. The XRD pattern of ZnO NPs from *C. scariosus* roots is shown in Figure 5. The diffraction peaks visible in the spectra are characteristic of ZnO NPs in their hexagonal wurtzite phase. The 2θ values of the observed Bragg reflections were 31.6°, 34.5°, 36.1°, 47.5°, 56.6°, 62.7°, 67.9°, and 69°, corresponding to (100), (002), (101), (102), (110), (103), (200), and (112) planes of the wurtzite phase (JCPDS Card No. 36-1451). Comparable trends were observed for ZnO NPs in several previous studies [61,62]. Our results are also in agreement with the study by Saemi et al. [63]. The observed peaks exhibit a considerable degree of crystallinity, as evidenced by their precision. No additional identifiable peaks belonging to foreign phases were identified, proving the existence of a pure ZnO NPs phase, with the exception of two weak points, 26.64° and 28.84° apart, which could be due to the plant extract. In this work, the crystallite or grain size of the green-produced ZnO NPs was determined by examining the XRD data. The Scherrer equation (Eq. 8) was used for this purpose, as follows:

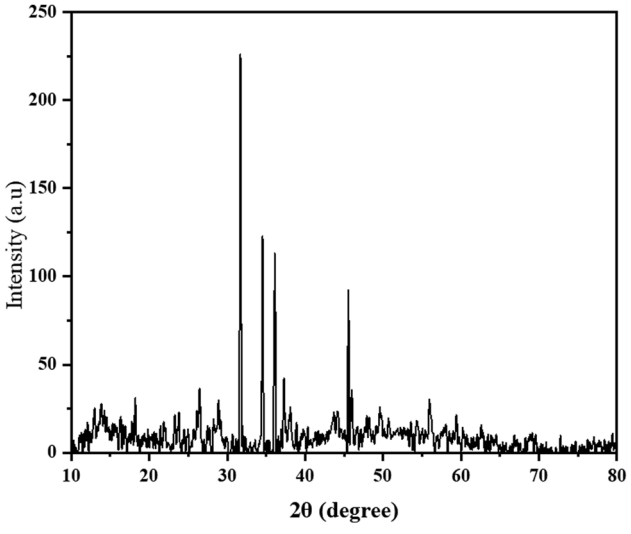

Figure 5: XRD patterns of the biogenic ZnO NPs.

$$D = K\lambda/\beta \cos\theta \tag{8}$$

where K is the Scherrer's standard and is equal to 0.9. The X-ray source used in this study has a wavelength of 0.15406 nm, which is given as λ. β represents the radian value of the FWHM of the analyzed peaks. In addition, θ stands for the orientation of the peak in radians. The analyzed ZnO NPs that were examined exhibited an average crystal size of 56.91 nm.

Based on the data from "Peak position (Table 3)," the 2θ (degrees), the interplanar distance (D in Å), and the Miller indices (hkl) for the different peaks "a" and "c" a hexagonal crystal structure of ZnO. The interplanar distance $dhkl$ for a hexagonal structure was defined by the following equation:

$$\frac{1}{d_{hkl}^2} = \frac{3}{4}\frac{(h^2 + hk + k^2)}{a^2}\frac{l^2}{c^2}$$

Using the above equation, the lattice parameters for the hexagonal structure of ZnO were precisely determined: a = 3.252 Å and c = 5.200 Å.

3.6 SEM

The surface morphology of the eco-friendly ZnO NPs was investigated by SEM [64]. Figure 6 (a–c, different magnifications and the particle histogram (d)) shows the surface

Table 3: Lattice parameters of ZnO wurtzite-hexagonal structure

Peak position 2θ (degree)	Interplanar spacing *D* (Å)	Miller indices (*hkl*)	Lattice parameter	
			Lattice constant	Lattice (Å)
31.6	2.829070446	100	$a = b$	3.252
34.5	2.597612156	002		
36.1	2.486067068	101		
47.5	1.912616589	102		
56.6	1.624803117	110	c	5.200
62.7	1.480592845	103		
67.9	1.3793061	200		
69	1.359977962	112		

morphology of the ZnO NPs at various magnifications. The SEM studies show that most of these particles have a semi-round shape, with an average diameter of 85.4 nm. Our findings are in agreement with those of a recently published study [65].

3.7 Characterization of ZnO NPs by (EDX)

The elemental characterization of ZnO NPs was performed using the energy-dispersive X-ray (EDX) technique. The EDX investigation, shown in Figure 7, demonstrated the existence of zinc and oxygen signals from ZnO NPs. Strong Zn signals were observed between 0 and 10 keV, which is consistent with recent literature [65,66]. The elemental composition of ZnO NPs was calculated and found to be 84.27% for zinc and 10.51% oxygen by weight. This composition suggests that the NPs are in a state of high purity.

3.8 DLS

3.8.1 Zeta sizer

The dynamic dispersion of light (DLS) method was used to estimate particle size using the Zetasizer Nano ZS (Malvern Panalytical). The device is capable of quantifying the dimensions of particles in liquid suspensions in the range of 0.1 nm to 12.3 µm. The device is capable of detecting a wide range of sample dispersion levels from a minimum of 0.00001% to a maximum of 40%. DLS is a method frequently used in colloid research to determine the particle size in a colloidal solution [67]. In this study, the average biogenic size of the synthesized ZnO NPs was calculated. The results of the DLS are shown in Figure 8(a). The data presented indicate an average particle size of 80 nm, which is consistent with the results of the SEM study, as illustrated in Figure 6. Figure 8(a) shows that the

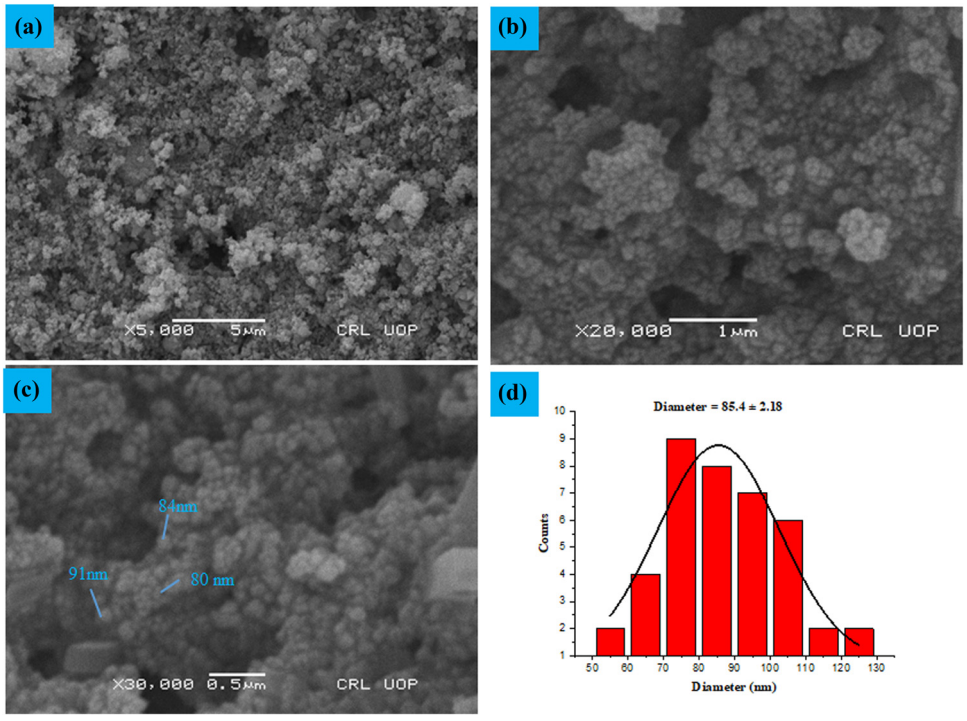

Figure 6: Surface morphology of ZnO NPs with different magnification.

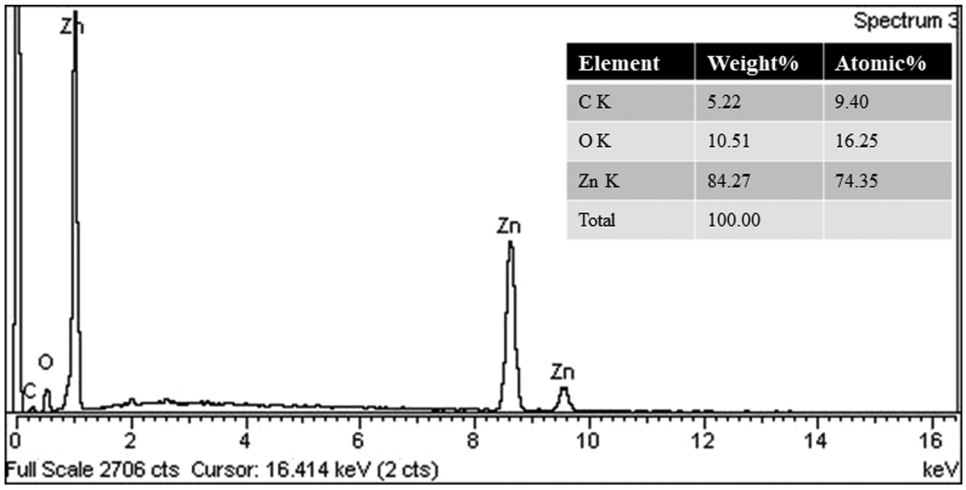

Figure 7: Elemental analysis of the biogenic synthesized ZnO NPs.

DLS size is bigger than the crystalline size determined by XRD. DLS is a faster and cheaper method to measure a large number of samples than XRD. DLS also provides a much larger value, which could be due to the hydrodynamic shell. The size of the hydrodynamic shell of a particle is also likely to be affected by its shape and roughness [67,68]. The influence of the physicochemical properties of a nanomaterial, including its dimensions, morphology, surface area, composition, and zeta potential, has a great impact on its biological activities [69].

3.8.2 Zeta potential

The zeta potentials of the biogenically synthesized ZnO NPs were measured by DLS analysis. The zeta potentials of the ZnO NPs were measured to be 51.2 mV, as shown in Figure 8(b). Coagulation occurs rapidly between 0 and ±5 mV of the zeta potential, whereas intermediate instability occurs between ±10 and ±30 mV, excellent stability between ±40 and ±60 mV, and exceptional stability above ±61 mV [70]. Therefore, the ZnO NPs synthesized by us have an overall excellent stability. Our results are in good agreement with previous literature [71].

3.9 Photocatalytic activity

3.9.1 Photocatalytic degradation of MO

The photocatalytic degradation activity of MO (anionic dye) by ZnO NPs was carried out under sunlight. It was observed that the dye underwent a color shift when exposed to sunlight. The ultraviolet-visible spectra of MO on ZnO NPs exposed to light are shown in Figure 9(a) at different time intervals. As time progressed, the dye was removed, as indicated by the decreasing intensity of the MO peak at λ_{max} of 464 nm. Figure 9(b) shows that MO degradation reached a peak value of 79.44% after 120 min of irradiation, which is consistent, with previous studies [13,72].

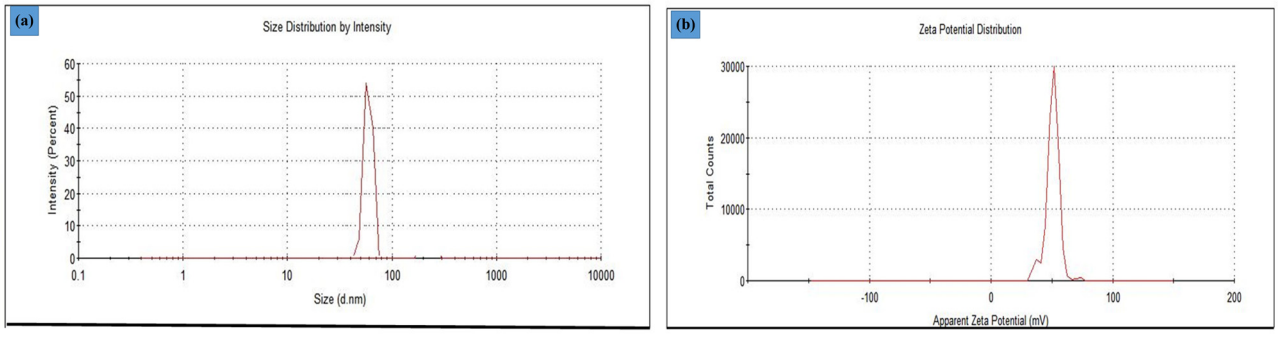

Figure 8: (a) Zeta sizer data of ZnO NPs, and (b) zeta potential of the synthesized ZnO NPs.

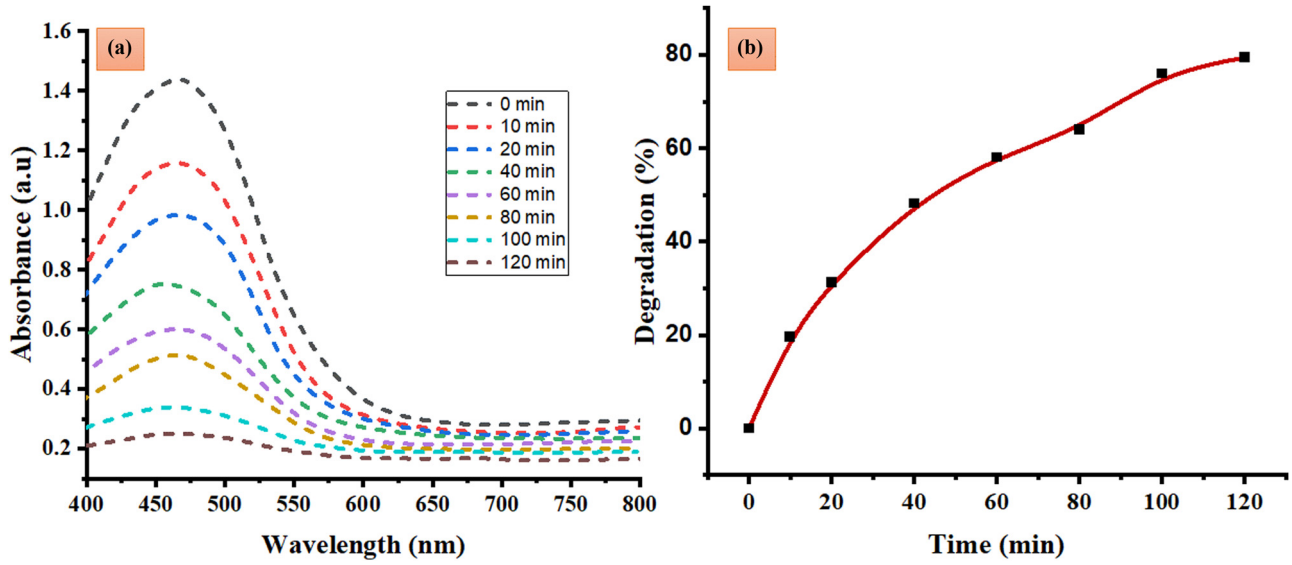

Figure 9: Photocatalytic degradation of MO: (a) ultraviolet-visible spectra of MO on ZnO NPs at different time intervals, and (b) degradation of MO in the presence of sunlight.

3.9.2 Photocatalytic degradation of methyl blue

Under sunlight irradiation, the photocatalytic degradation activity of MB (a cationic dye) by ZnO NPs was investigated. Over time, constant exposure to sunlight caused the deep blue color of the MB dye to change to a lighter shade of blue. Figure 10(a) illustrates the quantitative assessment of the dye's degradation by recording its UV-Vis spectra at various time intervals, including 0, 10, 20, 40, 60, 80, 100, and 120 min. From the recorded spectra, the intensity of the characteristic MB peak at λ_{max} of 665 nm keeps decreasing with time. This indicates that the dye concentration decreases, and the dye is degraded. The percentage degradation as a function of time is illustrated in Figure 10(b). 84.92% of the MB was degraded on the ZnO NPs catalyst within 2 h, when exposed to sunlight, as shown in this figure, which illustrates the progressive increase in percentage degradation over time. Our study showed comparable activities as previously reported [73,72].

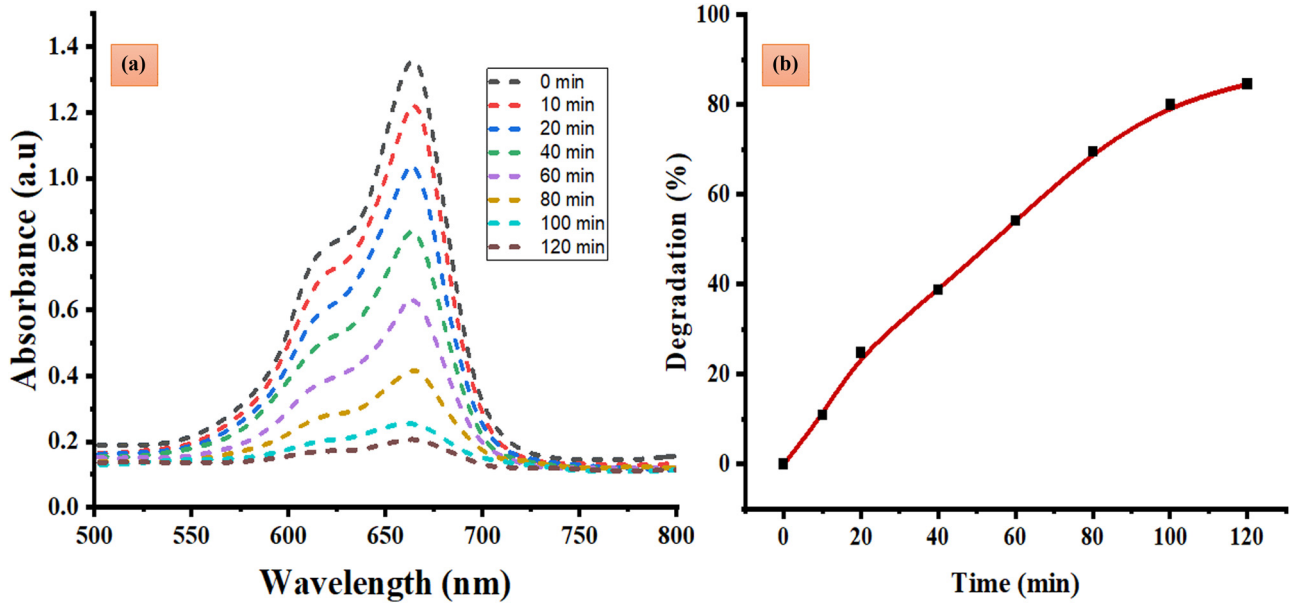

Figure 10: Photocatalytic degradation of methyl blue: (a) ultraviolet-visible spectra of MB on ZnO NPs at different time intervals, and (b) % degradation of methyl blue in the presence of sunlight.

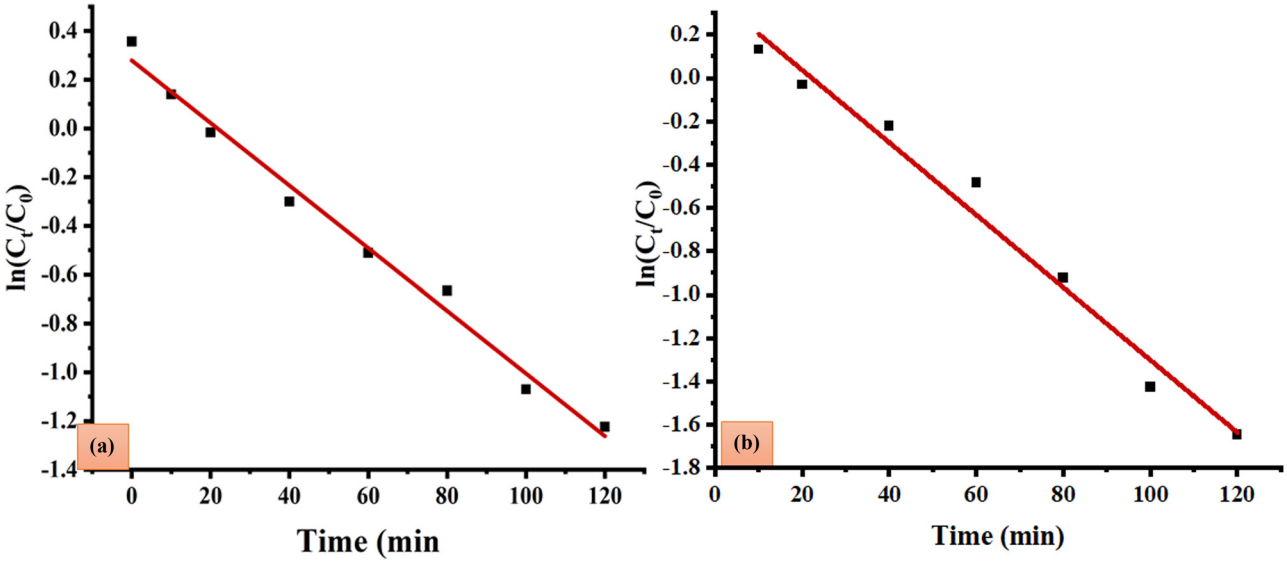

Figure 11: Kinetic study of $\ln(C_t/C_0)$ versus exposure time for first-order photocatalytic degradation of (a) MO and (b) methyl blue.

3.9.3 Kinetics rate of photodegradation of MO and MB on ZnO NPs

To investigate the kinetics of this photocatalytic process of MO and MB dyes, a plot of $\ln(C_t/C_0)$ versus exposure time was constructed (Figure 11a and b). The following equation (Eq. 9) was used to determine a linear relationship:

$$\ln\left(\frac{C_t}{C_0}\right) = -kt \tag{9}$$

where C_t is the concentration in the time interval t, C_0 is the concentration at time zero of the reaction, and k is the rate constant, which is determined by squaring the straight line. A high degree of linearity was found for both dyes, which shows that the photodegradation of MO and MB is based on first-order reaction kinetics. While the intercept value for MO is 0.279 ± 0.03 and has an R^2 value of 0.987, the intercept value for MB is 0.370 ± 0.076, with a correlation coefficient R^2 of 0.976. Similar kinetic rate values were found in a previous study on ZnO catalysts [13].

Table 4 summarizes the results of the comparison of the photocatalytic performance of the synthesized ZnO NPs with the results of a previous study that used the green synthesis technique for the photodegradation of MB and MO dyes. In this study, the ZnO NPs showed exceptional photocatalytic activity for both MB and MO dyes when exposed to sunlight.

3.9.4 Photocatalysts and photocatalytic mechanisms

The three types of semiconductor heterojunction configurations are based on the bandgap energies [77]. In the straddling-gap structure (type 1), semiconductor 2 has a larger negative capacitance (CB) and a larger positive valence (VB) than semiconductor 1. According to the principle of carrier transfer, electrons, and holes accumulate in semiconductor 1 at a lower E_g. Due to a smaller E_g, recombination of carriers may charge carrier recombination might occur, leading to a decrease in photocatalytic

Table 4: Compression of ZnO NP photocatalytic degradation with previous literature

Plant	Dye	Light source	Degradation efficiency (%)	Irradiation time (min)	Ref.
Sargassum muticum	MB	Natural sunlight	96	120	[74]
Cassia fistula	MO	UV	84	120	[75]
Wild olive	MO	Natural sunlight	92	90	[76]
O. europaea	MB	Natural sunlight	75	180	[13]
	MO		87		
ZnO NPs	MO	Natural sunlight	79.44	120	This work
	MB		84.92		

efficiency. Both the CB and VB of semiconductor 2 are more negatively correlated with each other in a staggered gap arrangement (type 2) than in semiconductor 1. Hence, holes migrate from semiconductor 1 to 2, while electrons migrate from semiconductor 2 to semiconductor 1. Due to the division of charge carriers between two semiconductors, type 2 offers superior electron-hole separation compared to type 1. In the third type of broken gap, semiconductor 2 has higher CB and VB than semiconductor 1 so, the interface of the semiconductor prevents electrons and holes from accessing their respective bands. This occurs due to the energy barrier that hinders the passage of charge carriers at the interface [78]. The type 2 semiconductor heterojunction structure is the most common of the three heterojunction structures. It enhances the photocatalytic reaction by preventing the recombination of charge carriers during electron transfer and promoting effective separation of the photogenerated electrons [79].

Dye-based model molecules for the photocatalytic activity of semiconductors can interact with degradation intermediates that absorb at the wavelength of the dye [80]. Sensitive dyes can be degraded due to photocatalysis, dye sensitization, or both [81]. Therefore, to evaluate the efficacy of the synthesized catalyst and to understand the degradation process, it is important to distinguish between these two effects. Based on previous research and our findings [82,13], Figure 12 shows the photocatalytic degradation mechanism of MB and MO on ZnO NPs. The photocatalytic degradation of ZnO typically involves the following processes (Eqs. 10–13):

$$\mathrm{ZnO} + h\nu \rightarrow \mathrm{ZnO} + \mathrm{e}^{-} + \mathrm{h}^{+} \tag{10}$$

$$\mathrm{O_2} + e^{-} \rightarrow \dot{\mathrm{O}}_2^{-} \tag{11}$$

$$\mathrm{h}^{+} + \mathrm{H_2O} \rightarrow \mathrm{OH}^{\cdot} + \mathrm{H}^{+} \tag{12}$$

$$\mathrm{OH}^{\cdot} + \dot{\mathrm{O}}_2^{-} + \text{organic dye(MO/MB)} \rightarrow \text{min eral acids} + \mathrm{CO_2} + \mathrm{H_2O}. \tag{13}$$

3.10 Antibacterial activity

Antibiotic resistance is a major problem in healthcare in emerging and industrialized countries. The increasing incidence of multidrug-resistant illnesses has a significant impact on current antibiotic therapy [70,59]. Hence, it is essential to explore alternative reservoirs of antimicrobial agents, such as plant-derived nanomaterials, which contain a variety of bioactive components with proven therapeutic attributes [59]. In the current situation, the use of environmentally benign techniques for the production of metallic NPs has been recognized as a highly beneficial development.

The current results indicate that biologically synthesized ZnO NPs have a remarkable antimicrobial impact on all bacterial strains tested in the study. This study showed significant antibacterial activity as evidenced by the inhibition zones for *Listeria monocytogenes* (ATCC 13932) (18 mm), *Staphylococcus epidermidis* (ATCC 12228) (20 mm), *Escherichia coli* (ATCC 10536) (16 mm), and *Bordetella bronchiseptica* (ATCC 4617) (14 mm). The negative control (DH_2O) showed no zone of inhibition when tested against these bacterial strains (see Figure 13). In addition, the biogenically produced ZnO NPs were found to have antibacterial activity almost equivalent to that of the positive control (ceftriaxone sodium). Zinc oxide has antibacterial activity because it has a stronger affinity for the amines and carboxyl groups that are frequently present on bacterial surfaces [61]. Due to its large surface area, ZnO NPs

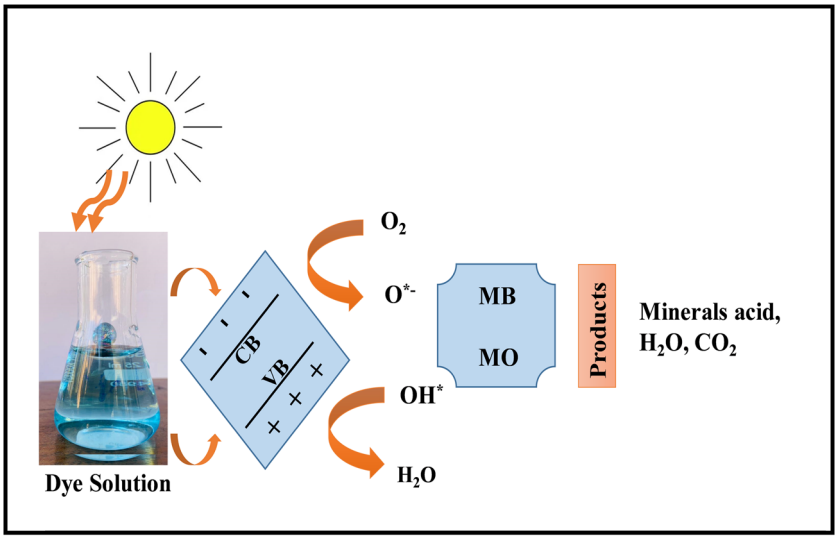

Figure 12: Possible photocatalytic degradation mechanism of MO and MB dyes.

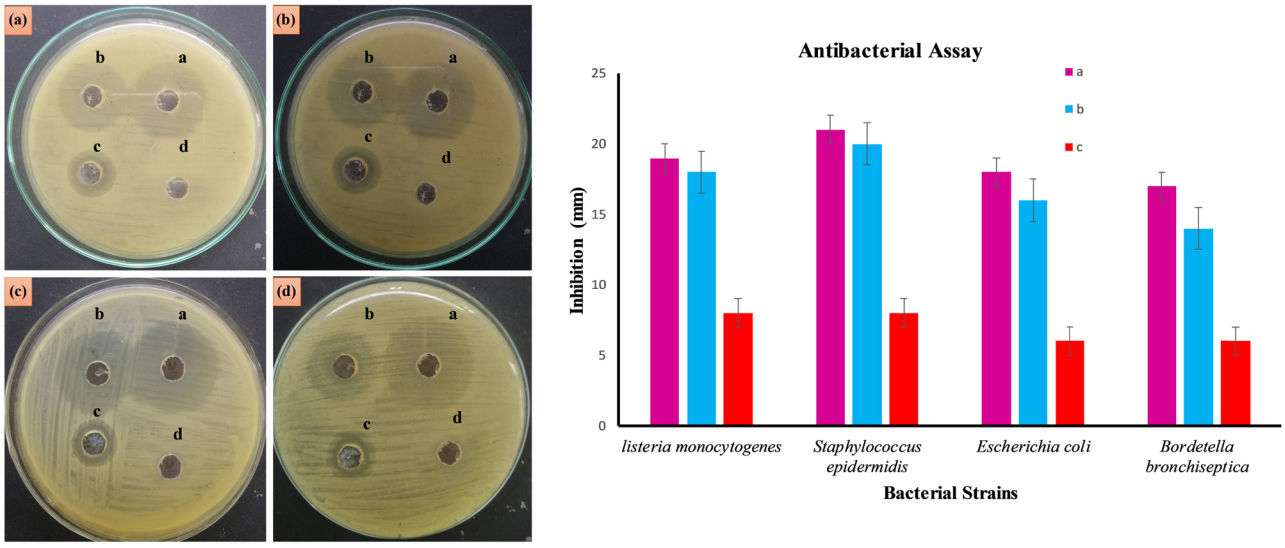

Figure 13: Antibacterial activity of the biogenic synthesized ZnO NPs (a) *Listeria monocytogenes* (ATCC 13932): ((a) positive control (19 mm), (b) ZnO NPs (18 mm), (c) plant root extract (8 mm), (d) negative control DH_2O (0 mm)). (b) *Staphylococcus epidermidis* (ATCC 12228): ((a) positive control (21 mm), (b) ZnO NPs (20 mm), (c) plant root extract (7 mm), (d) negative control DH_2O (0 mm)). (c) *Escherichia coli* (ATCC 10536): ((a) positive control (18 mm), (b) ZnO NPs (16 mm), (c) plant root extract (6 mm), (d) negative control DH_2O (0 mm)). (d) *Bordetella bronchiseptica* (ATCC 4617): ((a) positive control (17 mm), (b) ZnO NPs (14 mm), (c) plant root extract (6 mm), and (d) negative control DH_2O (0 mm)).

can have a larger antibacterial impact since they have greater possibilities to interact with microorganisms [83]. The resultant zinc ions may bind to DNA molecules, leading to cross-linking within and between strands and possibly destabilizing the helical structure of DNA [84]. Zinc ions also inhibit the biological processes that occur within bacterial cells [83]. It was shown that the antibacterial activity against Gram-positive bacteria was much higher than against Gram-negative bacteria. Gram-positive bacteria exhibit higher antibiotic resistance compared to Gram-negative bacteria owing to distinct structural differences in their cell walls [14,84]. Our results are in full agreement with several recent research studies [85,86,59]. Our results were also in agreement with the study by Rezazadeh et al. [87].

In this study, the broth dilution assay was used to determine the MIC against *Listeria monocytogenes* (ATCC#13932), *Staphylococcus epidermidis* (ATCC#12228), *Escherichia coli* (ATCC#10536) and *Bordetella bronchiseptica* (ATCC#4617). The values of the MIC are listed in Table 5. The results show that the MICs of ZnO NPs were 30 and 20 $\mu g \cdot mL^{-1}$ for *Listeria monocytogenes* (ATCC#13932), *Staphylococcus epidermidis* (ATCC#12228), and 40 and 70 $\mu g \cdot mL^{-1}$ for *Escherichia coli* (ATCC#10536) and *Bordetella bronchiseptica* (ATCC#4617), respectively. This indicates that the synthesized ZnO NPs effectively inhibit the growth of these four pathogens at relatively low concentrations. The current MIC data support previous results by showing that the Gram-negative bacterial strains *Escherichia coli* (ATCC#10536) and *Bordetella bronchiseptica* (ATCC#4617) are more resistant to ZnO NPs than the Gram-positive bacterial strains *Listeria monocytogenes* (ATCC#13932), and *Staphylococcus epidermidis* (ATCC#12228) [85]. This could be due to variations in the composition of their cell walls or to lipopolysaccharides that block the positive charges of ZnO NPs and reduce the susceptibility of *Escherichia coli* (ATCC#10536) and *Bordetella bronchiseptica* to ZnO NPs. The results show that ZnO NPs have a significant antibacterial effect on the investigated microbes. The enhanced antibacterial activity is attributed to the bioactive compounds present in the extract that cape the NPs and to the larger surface area of the NPs.

3.11 Antioxidant activity

3.11.1 Ferric-reducing antioxidant assay (FRAP)

The FRAP was used to measure antioxidant activity. A secondary antioxidant, ascorbic acid, was used to prepare the

Table 5: Inhibition zone (mm) and MIC of ZnO NPs

Bacterial strains	Zone of inhibition (mm)	MIC ($\mu g \cdot mL^{-1}$)
Listeria monocytogenes	18	30
Staphylococcus epidermidis	20	20
Escherichia coli	16	40
Bordetella bronchiseptica	14	70

Samples were analyzed at least in triplicate, and results are presented as mean ± standard deviation.

reference standard solution as it neutralizes free radicals and prevents further chain reactions. The hydroxyl groups in vitamin C are powerful antioxidants due to their polyhydroxyl structure and their capacity to neutralize free radicals [16]. The precipitated potassium ferrocyanide complex ($K_3Fe(CN)_6$) was removed with a TCA solution. The addition of $FeCl_3$ leads to the formation of a complex with a gradation of green to blue, a complex often referred to as "Blue Berlin." The reduction capacity of reduction was possibly an indicative feature of the antioxidant activity. The aim of the study was to evaluate antioxidants based on their ability to reduce ferric ions (Fe^{3+}) and ferrous ions (Fe^{2+}) ions. Figure 14(a) shows that the inhibition ranged from 33.7 to 66.29 µg (AAE µg·mL^{-1}) between 100 and 500 µL, as measured by an ascorbic acid standard curve. The synthesized NPs exhibit antioxidant capabilities associated with the stabilization of radicals through various processes, including direct proton transfer, electron transfer, hydrogen atom transfer, and sequential proton loss and electron transfer [88]. Overall, the biosynthesized ZnO NPs showed considerable antioxidant potential in ferric reduction antioxidant potential, which is confirmed by recent publications in the literature [44,88,89].

3.11.2 DPPH assay

The DPPH assay is a frequently used strategy for the quantitative assessment of the antioxidant potential of diverse substances. In this experimental design, DPPH serves as a resilient free radical that is involved in a chemical reaction with hydrogen or electrons provided by the sample. This interaction results in a striking color change from purple to yellow, as a diphenyl picrylhydrazine compound is formed. The antioxidant capabilities of ZnO NPs were evaluated in addition to ascorbic acid using a spectrophotometer (Shimadzu UV-1800 spectrophotometer). The results showing the percentage of radical scavenging activity (% RSA) are presented in Figure 14(b). The study showed that all concentrations tested exhibited significant radical scavenging capabilities. The ability to reduce free DPPH ions was highest (57.44 µg) (AAE µg·mL^{-1}) when the concentration was 500 µL (1 mg·mL^{-1}) for ZnO NPs. The synthesized ZnO NPs show greater free radical scavenging activity than the plant root extract and are almost similar to ascorbic acid. The findings presented here are in agreement with previous studies documented in the literature [90]. Numerous antioxidant chemicals are involved in the capping and

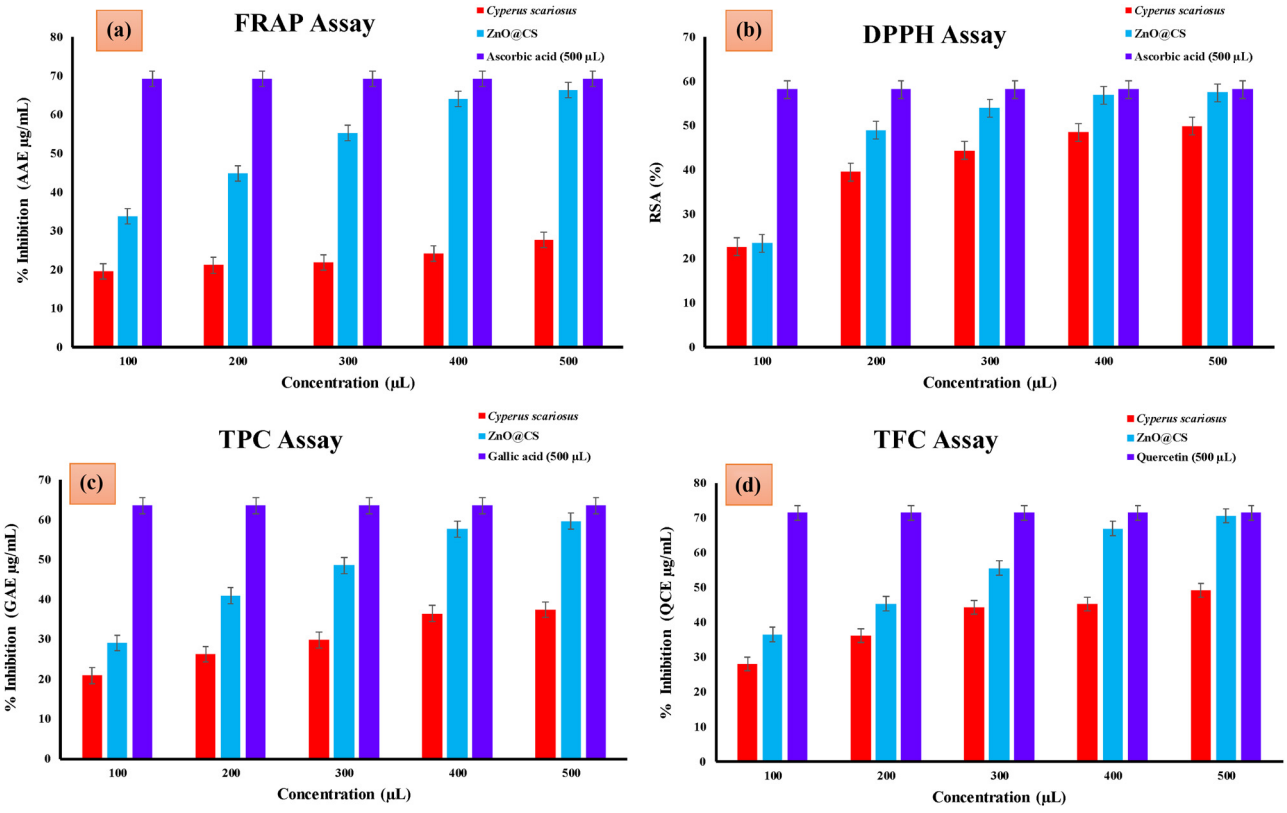

Figure 14: Antioxidant activities of biogenically synthesized ZnO NPs: (a) FRAP assay, (b) DPPH assay, (c) TPC assay, and (d) TFC assay.

Table 6: Determination of the percentage inhibition of protein denaturation

Concentration (µL) (1 mg·mL^{-1})	*C. scariosus* (% inhibition)	ZnO NPs (% inhibition)	Diclofenac sodium (500 µL) (1 mg·mL^{-1}) (% inhibition)
100	5.50	16.50	
200	8.14	54.49	
300	18.51	70.37	87.30159
400	31.21	83.06	
500	34.39	84.12	

Samples were analyzed in at least triplicate, and results are presented as mean ± standard deviation.

stabilization of NPs. The production of reactive oxygen species (ROS) by plant metabolic pathways under environmental stresses damages the membrane lipids, cell tissue, genome, and peptides. Researchers have found that flavonoids, terpenoids, and oxidative anti-stress regulators are some of the metabolically important substances that can contribute to the encapsulation and stabilization of NPs [64].

3.11.3 Total phenolic content (TPC)

The total phenolic content of the biogenic ZnO NPs and the *C. scariosus* extract was estimated using the Folin–Ciocalteu assay by establishing a standard curve with gallic acid (GA) based on the absorbance–concentration relationship. A linear calibration curve with $y = 0.0019x$ and R^2 of 0.9659 was determined from the standard curve with GA. It was shown that the ZnO NPs have a dose-dependent scavenging activity, as shown in Figure 14(c). The calibration curve equation indicated that the phenolic content of ZnO NPs at a concentration of 500 µL (57.63 GAE µg·mL^{-1}) was higher than that of the plant extract and compared to the standard.

3.11.4 TFC

The total content of flavonoids in the green synthesized ZnO NPs is illustrated in Figure 14(d). The calibration curve derived from the standard analysis (quercetin) was linear, with $y = 0.0002x$ and $R^2 = 0.9883$. The scavenging activity of ZnO NPs was found to be dose-dependent for the TFC. The calibration curve equation indicated that the ZnO NPs at a concentration of 500 µL exhibited the maximum TFC (70.59 µg QCE µg·mL^{-1}), which was greater than the plant extract (49.14 µg QCE µg·mL^{-1}) at the same concentration and almost comparable to the standard.

3.12 Anti-inflammatory activity

There is a common belief that medicinal plants represent a considerable reservoir of unique chemical compounds that can provide therapeutic advantages. Investigating the flora for novel anti-allergic medicines with traditional uses is a sensible research strategy. Inflammation can cause adverse effects and lead to hypersensitivity reactions that can be fatal and cause persistent organ damage [16]. Non-steroidal anti-inflammatory drugs (NSAIDs) are able to inhibit protein denaturation, a process that triggers the production of antigens and subsequently leads to the development of autoimmune diseases [91]. Protein denaturation is recognized as an important factor in the inflammatory response of the human body, particularly in the context of inflammatory diseases such as rheumatoid arthritis. The primary mode of action of NSAIDs involves the inhibition of protein denaturation [92]. Hence, it could be hypothesized that the observed anti-inflammatory effects of ZnO NPs are due to their ability to suppress protein denaturation. The anti-inflammatory effect of *C. scariosus* showed a dose-dependent response, as shown in Table 6. The maximum concentration (500 µg·mL^{-1}) of the synthesized ZnO NPs exhibited a value of 84.12%, whereas the minimum concentration (100 µg·mL^{-1}) of the synthesized ZnO NPs demonstrated a value of 16.50%. The results of this study show that the ZnO NPs were encapsulated by the secondary metabolites from the *C. scariosus* tuber root extract. Due to inhibition of neutrophils, the lysosomal components are at the site of inflammation, as demonstrated by the application of secondary metabolites from the plant extract. Following their release into the extracellular environment, bactericidal and proteolytic enzymes housed in the lysosomes contribute to exacerbating inflammation and causing tissue damage [72].

4 Conclusions

The present work provides a simple, rapid, cost-effective, and environmentally sustainable approach for the synthesis of biogenic ZnO NPs using *C. scariosus* root extract as a bio-reducing and capping agent. The synthesis of ZnO NPs was detected and confirmed by an absorption band at 366 nm, consistent with a localized surface plasmon

resonance (LSPR). The investigated ZnO NPs exhibit discrete photocatalytic degradation. Moreover, the synthesized ZnO NPs exhibit remarkable antibacterial potential against both Gram-positive and Gram-negative bacteria, as well as antioxidant and anti-inflammatory properties. Therefore, biogenically synthesized ZnO NPs have the potential to be used in environmental remediation and medical contexts, especially as an alternative therapy to marketed drugs, which are always associated with some side effects.

Acknowledgements: The authors extend their appreciation to the Researchers supporting project number (RSP2024R193), King Saud University, Riyadh, Saudi Arabia.

Funding information: Authors state no funding involved.

Author contributions: MA, SU, NA, MNH, MK, BM, and RS: Conceptualization, data curation, writing – original draft, formal analysis, investigation, and methodology; MNK, SW, MA, and AK: formal analysis, validation, visualization resources, writing – review and editing; M.A.J. and BA: data curation, formal analysis, software, visualization, writing – original draft, writing – review and editing. All authors contributed significantly, have read and agreed to the published version of the manuscript.

Conflict of interest: Authors state no conflict of interest.

Data availability statement: The datasets generated during and/or analyzed during the current study are available from the corresponding author on reasonable request.

References

[1] Scaccabarozzi AD, Basu A, Aniés F, Liu J, Zapata-Arteaga O, Warren R, et al. Doping approaches for organic semiconductors. Chem Rev. 2022;122:4420–92. doi: 10.1021/acs.chemrev.1c00581.

[2] Thomas SR, Pattanasattayavong P, Anthopoulos TD. Solution-processable metal oxide semiconductors for thin-film transistor applications. Chem Soc Rev. 2013;42:6910–23.

[3] Sridevi H, Bhat MR, Kumar PS, Kumar NM, Selvaraj R. Structural characterization of cuboidal α-Fe2O3 nanoparticles synthesized by a facile approach. Appl Nanosci. 2023;13:5605–13. doi: 10.1007/s13204-023-02780-y.

[4] Khan I, Saeed K, Khan I. Nanoparticles: Properties, applications and toxicities. Arab J Chem. 2019;12:908–31.

[5] Król A, Pomastowski P, Rafińska K, Railean-Plugaru V, Buszewski B. Zinc oxide nanoparticles: Synthesis, antiseptic activity and toxicity mechanism. Adv Colloid Interface Sci. 2017;249:37–52.

[6] Ajmal M, Ullah R, Muhammad Z, Khan MN, Kakar HA, Kaplan A, et al. Kinetin capped zinc oxide nanoparticles improve plant growth and ameliorate resistivity to polyethylene glycol (PEG)-induced drought stress in Vigna radiata (L.) R. Wilczek (Mung Bean). Molecules. 2023;28:5059.

[7] Ullah R, Bibi S, Khan MN, Al Mohaimeed AM, Naz Q, Kamal A. Application of bio-inspired gold nanoparticles as advanced nanomaterial in halt nociceptive pathway and hepatotoxicity via triggering antioxidation system. Catalysts. 2023;13:786.

[8] Irfan MI, Amjad F, Abbas A, Rehman MFU, Kanwal F, Saeed M, et al. Novel carboxylic acid-capped silver nanoparticles as antimicrobial and colorimetric sensing agents. Molecules. 2022;27:3363.

[9] Thi TUD, Nguyen TT, Thi YD, Thi KHT, Phan BT, Pham KN. Green synthesis of ZnO nanoparticles using orange fruit peel extract for antibacterial activities. RSC Adv. 2020;10:23899–907.

[10] Haq TU, Ullah R, Khan MN, Wahab S, Ali B, Kaplan A, et al. Phytodrug (Silymarin)-encapsulated cerium oxide nanoparticles (S-CeONPs) for in-vitro release, ameliorating antimicrobial, anticancer, anti-inflammatory and antioxidant potential. BioNanoSci. 2024. doi: 10.1007/s12668-023-01295-8.

[11] Alhadhrami A, Almalki AS, Adam AMA, Refat MS. Preparation of semiconductor zinc oxide nanoparticles as a photocatalyst to get rid of organic dyes existing factories in exchange for reuse in suitable purpose. Int J Electrochem Sci. 2018;13:6503–21.

[12] Krunks M, Katerski A, Dedova T, Acik IO, Mere A. Nanostructured solar cell based on spray pyrolysis deposited ZnO nanorod array. Sol Energy Mater Sol Cell. 2008;92:1016–9.

[13] Ghaffar S, Abbas A, Naeem-ul-Hassan M, Assad N, Sher M, Ullah S, et al. Improved photocatalytic and antioxidant activity of olive fruit extract-mediated ZnO nanoparticles. Antioxidants. 2023;12:1201.

[14] Jabbar A, Abbas A, Assad N, Naeem-ul-Hassan M, Alhazmi HA, Najmi A, et al. A highly selective Hg^{2+} colorimetric sensor and antimicrobial agent based on green synthesized silver nanoparticles using Equisetum diffusum extract. RSC Adv. 2023;13:28666–75.

[15] Ul Haq T, Ullah R, Khan MN, Nazish M, Almutairi SM, Rasheed RA. Seed priming with glutamic-acid-functionalized iron nanoparticles modulating response of Vigna radiata (L.) R. Wilczek (mung bean) to induce osmotic stress. Micromachines. 2023;14:736.

[16] Khan ZUR, Assad N, Naeem-ul-Hassan M, Sher M, Alatawi FS, Alatawi MS, et al. Aconitum lycoctonum L. (Ranunculaceae) mediated biogenic synthesis of silver nanoparticles as potential antioxidant, anti-inflammatory, antimicrobial and antidiabetic agents. BMC Chem. 2023;17:128. doi: 10.1186/s13065-023-01047-5.

[17] Moditswe C, Muiva CM, Juma A. Highly conductive and transparent Ga-doped ZnO thin films deposited by chemical spray pyrolysis. Optik. 2016;127:8317–25.

[18] Yuvakkumar R, Suresh J, Nathanael AJ, Sundrarajan M, Hong SI. Novel green synthetic strategy to prepare ZnO nanocrystals using rambutan (Nephelium lappaceum L.) peel extract and its antibacterial applications. Mater Sci Eng: C. 2014;41:17–27.

[19] Rojas S, Horcajada P. Metal–Organic Frameworks for the Removal of Emerging Organic Contaminants in Water. Chem Rev. 2020;120:8378–415. doi: 10.1021/acs.chemrev.9b00797.

[20] Bhole R, Gonsalves D, Murugesan G, Narasimhan MK, Srinivasan NR, Dave N, et al. Superparamagnetic spherical magnetite nanoparticles: synthesis, characterization and catalytic potential. Appl Nanosci. 2023;13:6003–14.

[21] Venkatesh N, Aravindan S, Ramki K, Murugadoss G, Thangamuthu R, Sakthivel P. Sunlight-driven enhanced photocatalytic activity of bandgap narrowing Sn-doped ZnO nanoparticles. Environ Sci Pollut Res. 2021;28:16792–803.

[22] Ghouri ZK, Elsaid K, Abdala A, Al-Meer S, Barakat NA. Surfactant/organic solvent free single-step engineering of hybrid graphene-Pt/TiO2 nanostructure: Efficient photocatalytic system for the treatment of wastewater coming from textile industries. Sci Rep. 2018;8:14656.
[23] Rajamohan S, Kumaravel V, Muthuramalingam R, Ayyadurai S, Abdel-Wahab A, Kwak BS, et al. Fe_3O_4–Ag_2WO_4: facile synthesis, characterization and visible light assisted photocatalytic activity. N J Chem. 2017;41:11722–30.
[24] Della-Flora A, Wilde ML, Lima D, Lima EC, Sirtori C. Combination of tertiary solar photo-Fenton and adsorption processes in the treatment of hospital wastewater: the removal of pharmaceuticals and their transformation products. J Environ Chem Eng. 2021;9:105666.
[25] Demir M, Taymaz BH, Sarıbel M, Kamış H. Photocatalytic degradation of organic dyes with magnetically separable PANI/Fe_3O_4 composite under both UV and visible-light irradiation. ChemistrySelect. 2022;7:e202103787. doi: 10.1002/slct.202103787.
[26] Velempini T, Prabakaran E, Pillay K. Recent developments in the use of metal oxides for photocatalytic degradation of pharmaceutical pollutants in water – A review. Mater Today Chem. 2021;19:100380.
[27] Hasanpour M, Hatami M. Photocatalytic performance of aerogels for organic dyes removal from wastewaters: Review study. J Mol Liq. 2020;309:113094.
[28] Samadi A, Xie M, Li J, Shon H, Zheng C, Zhao S. Polyaniline-based adsorbents for aqueous pollutants removal: A review. Chem Eng J. 2021;418:129425.
[29] Promdet P, Quesada-Cabrera R, Sathasivam S, Li J, Jiamprasertboon A, Guo J, et al. High defect nanoscale ZnO films with polar facets for enhanced photocatalytic performance. ACS Appl Nano Mater. 2019;2:2881–9. doi: 10.1021/acsanm.9b00326.
[30] Haspulat Taymaz B, Demir M, Kamış H, Orhan H, Aydoğan Z, Akıllı A. Facile and green synthesis of ZnO nanoparticles for effective photocatalytic degradation of organic dyes and real textile wastewater. Int J Phytoremediat. 2023;25:1306–17. doi: 10.1080/15226514.2022.2150142.
[31] Klinbumrung A, Panya R, Pung-Ngama A, Nasomjai P, Saowalakmeka J, Sirirak R. Green synthesis of ZnO nanoparticles by pineapple peel extract from various alkali sources. J Asian Ceram Soc. 2022;10:755–65. doi: 10.1080/21870764.2022.2127504.
[32] Nagajyothi PC, Cha SJ, Yang IJ, Sreekanth TVM, Kim KJ, Shin HM. Antioxidant and anti-inflammatory activities of zinc oxide nanoparticles synthesized using Polygala tenuifolia root extract. J Photochem Photobiol B: Biol. 2015;146:10–7.
[33] Ullah R, Jan SA, Khan MN, Nazish M, Kamal A, Kaplan A, et al. Euphorbia royleana Boiss derived silver nanoparticles and their applications as a nanotherapeutic agent to control microbial and oxidative stress-originated diseases. Pharmaceuticals. 2023;16:1413.
[34] Saratale RG, Benelli G, Kumar G, Kim DS, Saratale GD. Bio-fabrication of silver nanoparticles using the leaf extract of an ancient herbal medicine, dandelion (Taraxacum officinale), evaluation of their antioxidant, anticancer potential, and antimicrobial activity against phytopathogens. Environ Sci Pollut Res. 2018;25:10392–406.
[35] Jamdagni P, Khatri P, Rana JS. Green synthesis of zinc oxide nanoparticles using flower extract of Nyctanthes arbor-tristis and their antifungal activity. J King Saud Univ-Sci. 2018;30:168–75.
[36] Iqbal J, Abbasi BA, Yaseen T, Zahra SA, Shahbaz A, Shah SA, et al. Green synthesis of zinc oxide nanoparticles using Elaeagnus angustifolia L. leaf extracts and their multiple in vitro biological applications. Sci Rep. 2021;11:20988.
[37] Bandeira M, Giovanela M, Roesch-Ely M, Devine DM, da Silva Crespo J. Green synthesis of zinc oxide nanoparticles: A review of the synthesis methodology and mechanism of formation. Sustain Chem Pharm. 2020;15:100223.
[38] Kumar A, Chahal KK, Kataria D. A review on phytochemistry and pharmacological activities of Cyperus scariosus. J Pharmacogn Phytochem. 2017;6:510–7.
[39] Assad N, Naeem-ul-Hassan M, Ajaz Hussain M, Abbas A, Sher M, Muhammad G, et al. Diffused sunlight assisted green synthesis of silver nanoparticles using *Cotoneaster nummularia* polar extract for antimicrobial and wound healing applications. Nat Product Res. 2023;1–15. doi: 10.1080/14786419.2023.2295936.
[40] De Silva GO, Abeysundara AT, Aponso MMW. Extraction methods, qualitative and quantitative techniques for screening of phytochemicals from plants. Am J Essent Oils Nat Products. 2017;5:29–32.
[41] Mandal RK, Ghosh S, Majumder TP. Comparative study between degradation of dyes (MB, MO) in monotonous and binary solution employing synthesized bimetallic (Fe-CdO) NPs having antioxidant property. Results Chem. 2023;5:100788.
[42] Rajiv Chandar N, Agilan S, Thangarasu R, Muthukumarasamy N, Ganesh R. Influence of the annealing temperature on the formation of Mo 17 O 47 and MoO 3 nanoparticles and their Photocatalytic performances for the degradation of MB dye. J Mater Sci: Mater Electron. 2020;31:7378–88.
[43] Cockerill FR. Performance standards for antimicrobial susceptibility testing: twenty-first informational supplement. (No Title); 2011.
[44] Shobha N, Nanda N, Giresha AS, Manjappa P, Sophiya P, Dharmappa KK, et al. Synthesis and characterization of Zinc oxide nanoparticles utilizing seed source of Ricinus communis and study of its antioxidant, antifungal and anticancer activity. Mater Sci Eng: C. 2019;97:842–50.
[45] Orshiso TA, Zereffa EA, Murthy HCA, Demissie TB, Pardeshi O, Avhad LS, et al. Biosynthesis of *Artemisia abyssinica* leaf extract-mediated bimetallic ZnO–CuO nanoparticles: Antioxidant, anticancer, and molecular docking studies. ACS Omega. 2023;8:41039–53. doi: 10.1021/acsomega.3c01814.
[46] Demirgül K, Ozturk E. Changes in nutrients, energy, antioxidant and carotenoid levels of dried tomato (Lycopersicon esculentum) pomage treated with Aspergillus niger solid-state fermentation. Turkish J Agric-Food Sci Technol. 2021;9:701–8.
[47] Noreen H, Semmar N, Farman M, McCullagh JS. Measurement of total phenolic content and antioxidant activity of aerial parts of medicinal plant Coronopus didymus. Asian Pac J Trop Med. 2017;10:792–801.
[48] Do QD, Angkawijaya AE, Tran-Nguyen PL, Huynh LH, Soetaredjo FE, Ismadji S, et al. Effect of extraction solvent on total phenol content, total flavonoid content, and antioxidant activity of Limnophila aromatica. J Food Drug Anal. 2014;22:296–302.
[49] Gwatidzo L, Chowe L, Musekiwa C, Mukaratirwa-Muchanyereyi N. In vitro anti-inflammatory activity of Vangueria infausta: An edible wild fruit from Zimbabwe. Afr J Pharm Pharmacol. 2018;12:168–75.
[50] Kyene MO, Droepenu EK, Ayertey F, Yeboah GN, Archer M-A, Kumadoh D, et al. Synthesis and characterization of ZnO nanomaterial from Cassia sieberiana and determination of its anti-inflammatory, antioxidant and antimicrobial activities. Sci Afr. 2023;19:e01452.
[51] Neamah SA, Albukhaty S, Falih IQ, Dewir YH, Mahood HB. Biosynthesis of zinc oxide nanoparticles using Capparis spinosa L.

fruit extract: Characterization, biocompatibility, and antioxidant activity. Appl Sci. 2023;13:6604.
[52] Mutukwa D, Taziwa R, Khotseng LE. A review of the green synthesis of ZnO nanoparticles utilising Southern African indigenous medicinal plants. Nanomaterials. 2022;12:3456.
[53] Varadavenkatesan T, Lyubchik E, Pai S, Pugazhendhi A, Vinayagam R, Selvaraj R. Photocatalytic degradation of Rhodamine B by zinc oxide nanoparticles synthesized using the leaf extract of Cyanometra ramiflora. J Photochem Photobiol B: Biol. 2019;199:111621.
[54] Dobrucka R, Długaszewska J. Biosynthesis and antibacterial activity of ZnO nanoparticles using Trifolium pratense flower extract. Saudi J Biol Sci. 2016;23:517–23.
[55] Kiro A, Bajpai J, Bajpai AK. Designing of silk and ZnO based antibacterial and noncytotoxic bionanocomposite films and study of their mechanical and UV absorption behavior. J Mech Behav Biomed Mater. 2017;65:281–94.
[56] Koli K, Rohtela K, Meena D. Comparative Study and Analysis of Structural and Optical Properties of Zinc Oxide Nanoparticles using Neem and Mint Extract prepared by Green synthesis method. IOP Conference Series: Materials Science and Engineering. Vol. 1248. IOP Publishing; 2022. p. 012065.
[57] Balcha A, Yadav OP, Dey T. Photocatalytic degradation of methylene blue dye by zinc oxide nanoparticles obtained from precipitation and sol-gel methods. Environ Sci Pollut Res. 2016;23:25485–93.
[58] Vinayagam R, Pai S, Varadavenkatesan T, Pugazhendhi A, Selvaraj R. Characterization and photocatalytic activity of ZnO nanoflowers synthesized using Bridelia retusa leaf extract. Appl Nanosci. 2023;13:493–502. doi: 10.1007/s13204-021-01816-5.
[59] Alikord M, Shariatifar N, Saraji M, Jahed Khaniki G, Hosseini H, Fazeli M. Biosynthesis of zinc oxide nanoparticles using fermented table olive extract: A novel and green approach with potential applications. BioNanoScience. 2023;1–16.
[60] Vahidi A, Vaghari H, Najian Y, Najian MJ, Jafarizadeh-Malmiri H. Evaluation of three different green fabrication methods for the synthesis of crystalline ZnO nanoparticles using Pelargonium zonale leaf extract. Green Process Synth. 2019;8:302–8. doi: 10.1515/gps-2018-0097.
[61] Motazedi R, Rahaiee S, Zare M. Efficient biogenesis of ZnO nanoparticles using extracellular extract of Saccharomyces cerevisiae: Evaluation of photocatalytic, cytotoxic and other biological activities. Bioorg Chem. 2020;101:103998.
[62] Hashemi S, Asrar Z, Pourseyedi S, Nadernejad N. Green synthesis of ZnO nanoparticles by Olive (*Olea europaea*). IET Nanobiotechnol. 2016;10:400–4. doi: 10.1049/iet-nbt.2015.0117.
[63] Saemi R, Taghavi E, Jafarizadeh-Malmiri H, Anarjan N. Fabrication of green ZnO nanoparticles using walnut leaf extract to develop an antibacterial film based on polyethylene–starch–ZnO NPs. Green Process Synth. 2021;10:112–24. doi: 10.1515/gps-2021-0011.
[64] Faisal S, Jan H, Shah SA, Shah S, Khan A, Akbar MT, et al. Green synthesis of zinc oxide (ZnO) nanoparticles using aqueous fruit extracts of *Myristica fragrans*: Their characterizations and biological and environmental applications. ACS Omega. 2021;6:9709–22. doi: 10.1021/acsomega.1c00310.
[65] Pillai AM, Sivasankarapillai VS, Rahdar A, Joseph J, Sadeghfar F, Rajesh K, et al. Green synthesis and characterization of zinc oxide nanoparticles with antibacterial and antifungal activity. J Mol Struct. 2020;1211:128107.
[66] Khan SB, Khan MI, Nisar J. Microwave-assisted green synthesis of pure and Mn-doped ZnO nanocomposites: In vitro antibacterial assay and photodegradation of methylene blue. Front Mater. 2022;8:710155.
[67] Yedurkar S, Maurya C, Mahanwar P. Biosynthesis of zinc oxide nanoparticles using ixora coccinea leaf extract – a green approach. Open J Synth Theory Appl. 2016;5:1–14.
[68] Barzinjy AA, Azeez HH. Green synthesis and characterization of zinc oxide nanoparticles using Eucalyptus globulus Labill. leaf extract and zinc nitrate hexahydrate salt. SN Appl Sci. 2020;2:991. doi: 10.1007/s42452-020-2813-1.
[69] Duffin R, Tran L, Brown D, Stone V, Donaldson K. Proinflammogenic effects of low-toxicity and metal nanoparticles in vivo and in vitro: Highlighting the role of particle surface area and surface reactivity. Inhalation Toxicol. 2007;19:849–56. doi: 10.1080/08958370701479323.
[70] Kumar A, Dixit CK. Methods for characterization of nanoparticles. Advances in nanomedicine for the delivery of therapeutic nucleic acids. Elsevier; 2017. p. 43–58.
[71] Nehru L, Kandasamy GD, Sekar V, Alshehri MA, Panneerselvam C, Alasmari A, et al. Green synthesis of ZnO-NPs using endophytic fungal extract of *Xylaria arbuscula* from *Blumea axillaris* and its biological applications. Artif Cells Nanomed Biotechnol. 2023;51:318–33. doi: 10.1080/21691401.2023.2232654.
[72] Govindappa M, Naga SS, Poojashri MN, Sadananda TS, Chandrappa CP. Antimicrobial, antioxidant and in vitro anti-inflammatory activity of ethanol extract and active phytochemical screening of Wedelia trilobata (L.) Hitchc. J Pharmacogn Phytother. 2011;3:43–51.
[73] Siripireddy B, Mandal BK. Facile green synthesis of zinc oxide nanoparticles by Eucalyptus globulus and their photocatalytic and antioxidant activity. Adv Powder Technol. 2017;28:785–97.
[74] Bopape DA, Motaung DE, Hintsho-Mbita NC. Green synthesis of ZnO: Effect of plant concentration on the morphology, optical properties and photodegradation of dyes and antibiotics in wastewater. Optik. 2022;251:168459.
[75] Karnan T, Selvakumar SAS. Biosynthesis of ZnO nanoparticles using rambutan (Nephelium lappaceumL.) peel extract and their photocatalytic activity on methyl orange dye. J Mol Struct. 2016;1125:358–65.
[76] Algarni TS, Abduh NA, Aouissi A, Al Kahtani A. Photodegradation of methyl orange under solar irradiation on Fe-doped ZnO nanoparticles synthesized using wild olive leaf extract. Green Process Synth. 2022;11:895–906.
[77] Pirhashemi M, Habibi-Yangjeh A, Pouran SR. Review on the criteria anticipated for the fabrication of highly efficient ZnO-based visible-light-driven photocatalysts. J Ind Eng Chem. 2018;62:1–25.
[78] Zhang L, Jaroniec M. Toward designing semiconductor-semiconductor heterojunctions for photocatalytic applications. Appl Surf Sci. 2018;430:2–17.
[79] Koe WS, Lee JW, Chong WC, Pang YL, Sim LC. An overview of photocatalytic degradation: photocatalysts, mechanisms, and development of photocatalytic membrane. Environ Sci Pollut Res. 2020;27:2522–65.
[80] Minero C, Pellizzari P, Maurino V, Pelizzetti E, Vione D. Enhancement of dye sonochemical degradation by some inorganic anions present in natural waters. Appl Catal B: Environ. 2008;77:308–16.

[81] Barbero N, Vione D. Why dyes should not be used to test the photocatalytic activity of semiconductor oxides. Env Sci Technol. 2016;50:2130–1. doi: 10.1021/acs.est.6b00213.
[82] Trandafilović LV, Jovanović DJ, Zhang X, Ptasińska S, Dramićanin MD. Enhanced photocatalytic degradation of methylene blue and methyl orange by ZnO: Eu nanoparticles. Appl Catal B: Environ. 2017;203:740–52.
[83] Chikkanna MM, Neelagund SE, Rajashekarappa KK. Green synthesis of zinc oxide nanoparticles (ZnO NPs) and their biological activity. SN Appl Sci. 2019;1:117. doi: 10.1007/s42452-018-0095-7.
[84] Kim J-H, Cho H, Ryu S-E, Choi M-U. Effects of metal ions on the activity of protein tyrosine phosphatase VHR: highly potent and reversible oxidative inactivation by Cu^{2+} ion. Arch Biochem Biophys. 2000;382:72–80.
[85] Lara HH, Ayala-Núñez NV, Ixtepan Turrent L, del C, Rodríguez Padilla C. Bactericidal effect of silver nanoparticles against multidrug-resistant bacteria. World J Microbiol Biotechnol. 2010;26:615–21.
[86] MuthuKathija M, Badhusha MSM, Rama V. Green synthesis of zinc oxide nanoparticles using Pisonia Alba leaf extract and its antibacterial activity. Appl Surf Sci Adv. 2023;15:100400.
[87] Rezazadeh NH, Buazar F, Matroodi S. Synergistic effects of combinatorial chitosan and polyphenol biomolecules on enhanced antibacterial activity of biofunctionalized silver nanoparticles. Sci Rep. 2020;10:19615.
[88] Boulmokh Y, Belguidoum K, Meddour F, Amira-Guebailia H. Investigation of antioxidant activity of epigallocatechin gallate and epicatechin as compared to resveratrol and ascorbic acid: Experimental and theoretical insights. Struct Chem. 2021;32:1907–23.
[89] Soleimani-Amiri S, Hossaini Z, Azizi Z. Synthesis and investigation of biological activity of new oxazinoazepines: Application of Fe_3O_4/CuO/ZnO@MWCNT magnetic nanocomposite in reduction of 4-nitrophenol in water. Polycycl Aromat Compd. 2023;43:2938–59. doi: 10.1080/10406638.2022.2058969.
[90] Gur T, Meydan I, Seckin H, Bekmezci M, Sen F. Green synthesis, characterization and bioactivity of biogenic zinc oxide nanoparticles. Environ Res. 2022;204:111897.
[91] Sangeetha G, Vidhya R. In vitro anti-inflammatory activity of different parts of Pedalium murex (L.). Inflammation. 2016;4:31–6.
[92] Sharifi-Rad M, Pohl P, Epifano F, Álvarez-Suarez JM. Green synthesis of silver nanoparticles using Astragalus tribuloides delile. root extract: Characterization, antioxidant, antibacterial, and anti-inflammatory activities. Nanomaterials. 2020;10:2383.